NEA/NSC/DOC(94)21
INDC(Ger)-039/LN
Jül-2950

PROGRESS REPORT ON NUCLEAR DATA RESEARCH IN THE FEDERAL REPUBLIC OF GERMANY

for the Period April 1, 1993 to March 31, 1994

August 1994

Edited by
S.M. Qaim
Forschungszentrum Jülich GmbH
Institut für Nuklearchemie
Jülich, Federal Republic of Germany

NEA/NSC/DOC(94)21
INDC(Ger)-039/LN

Jül-2950
Berichte des Forschungszentrums Jülich; 2950

Edited by: S.M. Qaim
Forschungszentrum Jülich GmbH
Institut für Nuklearchemie
Jülich, Federal Republic of Germany

FOREWORD

As in previous years, this report has been prepared to promote the exchange of nuclear data research information between the Federal Republic of Germany and other member states of OECD/NEA and IAEA. It covers progress reports from KfK Karlsruhe, KFA Jülich, the universities of Dresden, Hannover, Köln, Mainz, Marburg, München as well as from PTB Braunschweig. The emphasis in the work reported here is on measurement, compilation and evaluation of nuclear data for pure and applied science programmes, such as those relevant to fission- and fusion-reactor technology, radioactive waste management, accelerator shielding and development, astrophysics research, cosmogenic and meteoritic investigations, production of medically important radioisotopes, etc.

In a recent publication entitled: "A Strategic View On Nuclear Data Needs", the NEA drew attention to the changing trends in nuclear data research and future needs. In Germany the nuclear data activities have been undergoing a shift from "traditional" area of fission reactor technology to other applications. The present report vividly reflects this changing trend.

Each contribution is presented under the laboratory heading from where the work is reported. The names of other participating laboratories are also mentioned. When the work is relevant to the World Request List for Nuclear Data, WRENDA 93/94 (INDC(SEC)-104/U+G), the corresponding identification numbers are given.

Jülich, August 1994 S.M. Qaim

CONTENTS

INSTITUT FÜR KERN- UND TEILCHENPHYSIK
TECHNISCHE UNIVERSITÄT DRESDEN

Page

KERNFORSCHUNGSZENTRUM KARLSRUHE
INSTITUT FÜR KERNPHYSIK

1. THE s-ABUNDANCES OF THE TIN ISOTOPES

K. Wisshak, Ch. Theis, K. Guber, F. Voß, F. Käppeler,
L. Kazakov[1], N. Kornilov[1]

Of the three rare tin isotopes ^{112}Sn, ^{114}Sn and ^{115}Sn only the even isotopes are considered to be produced significantly by the p-process, while ^{115}Sn is assumed to originate mainly from the s- and r-processes with only a minor p-process contribution. In the mass region $112 < A < 116$ the s- and r-process flows are complicated by numerous low lying isomers that result in temperature-dependent branchings. The main s-process path proceeds via ^{114}Cd - ^{115}Cd - ^{115}In - ^{116}In - ^{116}Sn and bypasses ^{115}Sn. At low temperatures, the 336.24 keV isomer of ^{115}In is populated significantly in the s-process. This isomer decays with a 5 % probability to ^{115}Sn, but at high temperatures ^{115}In is thermalized, resulting in a strong depopulation of the isomer. Accordingly, the classical model with temperatures of $\sim 3 \times 10^8$ K yields almost no s-process contribution to ^{115}Sn.

The quantitative investigation of the production of ^{115}Sn is hampered by the lack of detailed cross section data. So far, Timokhov et al. (1989) reported neutron capture cross sections for the tin isotopes for energies above 20 keV with an accuracy of ~ 5 % for ^{115}Sn and ~ 7 % for ^{116}Sn. At lower energies, which become relevant in stellar models, only theoretical estimates exist for ^{115}Sn. For the reliable for determination of the s-process contribution an accuracy of 1-2 % for the capture cross section of the s-only isotope ^{116}Sn is required.

Therefore, the (n,γ) cross sections for $^{114-118}$Sn and ^{120}Sn were investigated with the Karlsruhe 4π BaF_2 detector. For a description of the experimental setup see the contribution of Wisshak et al. (1993 and references therein). The capture cross sections of the tin isotopes were measured relative to gold as a standard and using isotopically enriched metallic samples. Two runs with maximum neutron energies of 100 keV and 200 keV were perfomed with the 4π BaF_2 detector operated as a gamma-ray calorimeter. In a third run the capture cascades were detected with an ADC system in order to determine the fraction of unobserved capture events on the basis of experimental information.

All events were sorted in two-dimensional spectra according to sum energy and time of flight (TOF) with the multiplicity as an additional parameter. The sample-independent background was determined from the spectrum measured with an empty position in the sample ladder. The spectra were then corrected for isotopic impurities and for the background due to sample scattered neutrons. This scattering correction is obtained as a function of TOF and yields a reliable determination of the capture cross sections at all

[1]IPPE Obninsk, Russia

neutron energies.

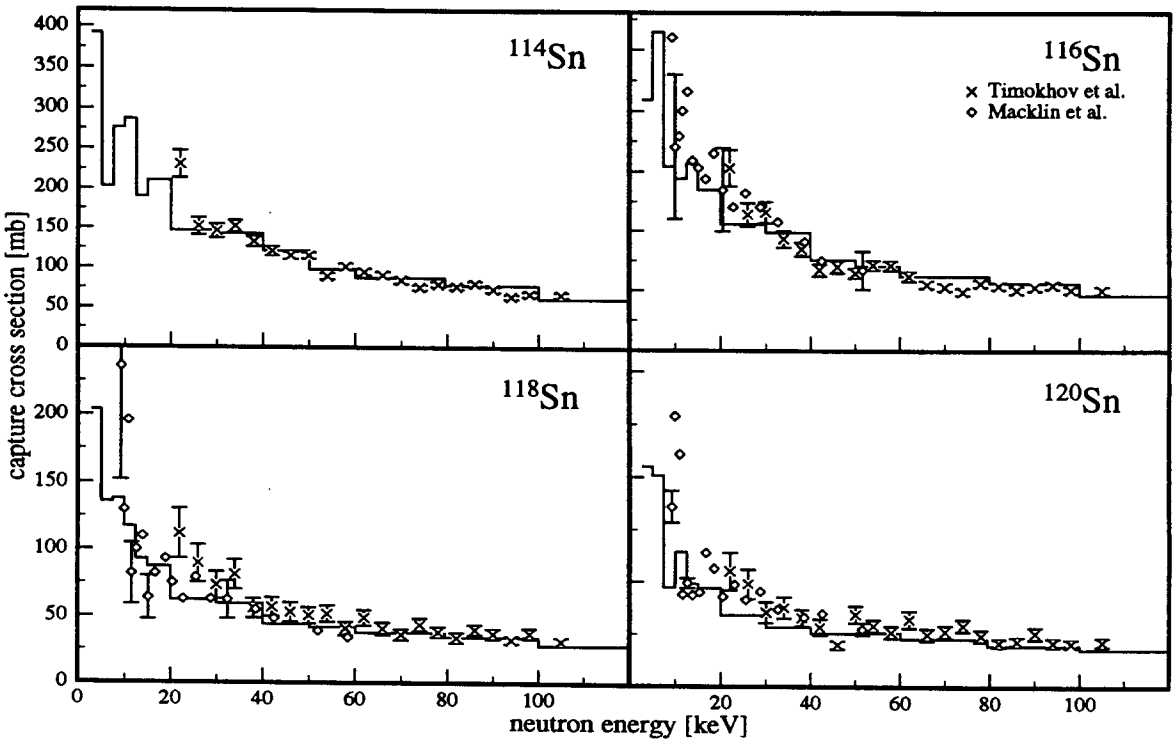

Figure 1: Comparison of the present capture cross sections (solid lines) with previous data

Preliminary cross sections for the even isotopes are compared in Figure 1 with the results of Macklin et al. (1962) and of Timokhov et al. (1989). Based on the experience from previous measurements an uncertainty of $\sim 2\,\%$ is expected for the present data.
With these new cross sections for a series of stable tin isotopes the s–process flow in the Cd–In–Sn region can be investigated with improved accuracy. In this way, the s–process contribution to ^{115}Sn as well as to ^{113}In can be studied for various s–process models.

R. L. Macklin, T. Inada and J. H. Gibbons 1962, *AEC, Washington Reports to the NCSAG* **1041**, 30 (Data from EXFOR 11981)

V. Timokhov, M. Bokhovo, A. Isakov, L. Kazakov, V. Kononov, G. Mantorov, E. Poletaev and V. Pronyaev 1989, *Sov. J. Nucl. Phys.* **50**, 375

K. Wisshak, K. Guber, F. Voß, F. Käppeler and G. Reffo 1993, *Phys. Rev.* **C48**, 1401

2. STELLAR NEUTRON CAPTURE CROSS SECTIONS OF THE Ba ISOTOPES

F. Voß, K. Wisshak, K. Guber, F. Käppeler, G. Reffo[1]

The neutron capture cross sections of ^{134}Ba, ^{135}Ba, ^{136}Ba, and ^{137}Ba were measured in the energy range from 5 to 225 keV . Neutrons were produced via the ^{7}Li(p,n)^{7}Be reaction by

[1]ENEA, Laboratorio Dati Nucleari, Viale Ercolani 8, I–40138 Bologna, Italy

Table 1: Maxwellian averaged neutron capture cross sections at kT = 30 keV compared to previous evaluations

Isotope	$< \sigma v > / v_T$ (mbarn)		
	This Work	Bao and Käppeler (1987)	Beer, Voss, and Winters (1992)
^{134}Ba	176.3 ± 5.6	221 ± 35	221 ± 34
^{135}Ba	455.0 ± 15.0	457 ± 80	295 ± 59
^{136}Ba	62.0 ± 2.1	69 ± 10	60 ± 10
^{137}Ba	76.9 ± 2.9	57 ± 10	52 ± 10

bombarding metallic Li targets with a pulsed proton beam. Capture events were registered with the Karlsruhe 4π BaF_2 detector. The cross section ratios were determined with an overall uncertainty of ~3%, an improvement by factors of five to eight compared to existing data. Severe discrepancies were found with respect to previous results. As a new possibility in time of flight experiments, isomeric cross section ratios could be determined for ^{135}Ba, ^{136}Ba, and ^{137}Ba. Maxwellian averaged neutron capture cross sections were calculated for thermal energies between kT = 10 keV and 100 keV. In Table 1, the values for kT=30 keV are compared with previous compilations.

These stellar cross sections are important for s–process analyses concerning the s–process branching at ^{134}Cs, which is defined by the s–only isotopes ^{134}Ba and ^{136}Ba. This branching yields information on the s–process temperature, indicating values around T_8 = 2. The new cross sections are also important for the interpretation of barium isotopic anomalies, which were recently discovered in SiC grains of carbonaceous chondrite meteorites. Together with the results from previous experiments on tellurium and samarium, a general improvement of the $N_s<\sigma>$ systematics in the mass range A = 120 to 150 is achieved. This yields a more reliable separation of s– and r–process contributions for comparison with stellar observations, but reveals a 20% discrepancy with respect to the solar barium abundance.

Z. Y. Bao and F. Käppeler 1987, *Atomic Data Nucl. Data Tables* **36**, 411
H. Beer, F. Voß and R. R. Winters 1992, *Ap. J. Suppl.* **80**, 403

3. ACTIVATION MEASUREMENTS ON ^{146}Nd, ^{148}Nd, AND ^{150}Nd

K. A. Toukan[1], K. Debus[2], F. Käppeler

The neutron capture cross sections of ^{146,148,150}Nd have been determined relative to that of gold by means of the activation method. The samples were irradiated in a quasi–stellar neutron spectrum for kT = 25 keV using the ^{7}Li(p,n)^{7}Be reaction near threshold. Variation of the experimental conditions in different activations and the use of different samples allowed to determine the necessary corrections and to evaluate systematic uncertainties quantitatively. The resulting stellar cross sections can be given with uncertainties of 6%,

[1]College of Engineering and Technology, The University of Jordan, Amman, Jordan
[2]University of Heidelberg

an improvement by factors 2 to 4 compared to the previously recommended values. The new data together with a set of improved cross sections for the unstable branch point nuclei ^{147}Nd, ^{147}Pm, and ^{148}Pm, which were obtained by statistical model calculations, provide for a quantitative discussion of the s–process flow in the Nd–Pm–Sm region. This is of particular interest for the determination of the neutron density during stellar helium burning.

4. STELLAR (n,γ) CROSS SECTIONS OF UNSTABLE s–PROCESS NUCLEI*

S. Jaag, F. Käppeler

When the s–process nucleosynthesis path encounters an unstable isotope with a half–life comparable to the neutron capture time, the resulting branching of the reaction flow leads to an abundance pattern that carries information on the physical parameters of the stellar plasma. The (n,γ) cross sections of these isotopes are important for the interpretation of the respective branchings. While the neutron capture cross sections of the stable isotopes are known with good accuracy, there is a complete lack of experimental data for the radioactive branch point isotopes. This contribution describes activation measurements on the unstable targets, ^{155}Eu and ^{163}Ho.

The activation technique offers the advantage of very good sensitivity. This is important for measurements on radioactive target because only a small quantity of sample material is needed. However, the number of accessible isotopes is limited due to the requirement that also the 'produced' nuclei must be unstable.

The branchings at ^{154}Eu ($t_{1/2}$ = 8.8 yr) and ^{155}Eu ($t_{1/2}$ = 4.96 yr) can both be considered as s–prosess thermometers. But while the ^{154}Eu branching is characterized by the s–only isotope ^{154}Gd, the ^{155}Eu branching is obscured by the r–process contribution to ^{155}Gd. For experimental reasons, there is almost no chance to measure the ^{154}Eu cross section directly. Therefore, the motivation of the present measurement was, to use the experimental value for ^{155}Eu to improve the statistical model calculation of the more important ^{154}Eu cross section.

In order to achieve the required isotopic purity, the ^{155}Eu–sample was breeded in a reactor from an enriched batch of 1.55 g ^{154}Sm. Before, this batch had to be purified chemically in order to reduce small but disturbing impurities from other rare earth elements to an acceptable level. In this respect, an 0.013 % Eu contamination was the most critical point, since this gives rise to an interfering background from ^{152}Eu and ^{154}Eu activities in the later activation. This Eu contamination could be reduced by a factor 400 by means of the ion exchange technique.

The purified batch of ^{154}Sm was exposed to a thermal neutron flux of $10^{13}\,\mathrm{sec}^{-1}\,\mathrm{cm}^{-2}$ in the reactor of the DKFZ Heidelberg for 90 min. The so produced ^{155}Eu was then concentrated in a second step, using the same ion exchange technique. The final sample contained $3.34 \cdot 10^{14}$ atoms of ^{155}Eu, which was determined via the activity. This ^{155}Eu was imbedded in a remaining macroscopic quantity of Sm_2O_3, which was pressed to a pellet and canned in a thin walled graphite box. The final activation was started after a waiting time of 220 days to allow all of the coproduced ^{156}Eu to decay ($t_{1/2}$ = 15.6 d).

*PhD thesis, S. Jaag (1994), University of Karlsruhe

The activation was performed at the Karlsruhe Van de Graaff accelerator using a quasi–stellar neutron spectrum of the ^{7}Li(p,n)^{7}Be reaction (Ratynski and Käppeler 1988). The ^{155}Eu–sample was sandwiched between two gold foils for flux normalization and mounted directly on the Li–target. The irradiation lasted for 17 days at an average neutron flux of $3 \cdot 10^{9}\,\mathrm{sec}^{-1}\,\mathrm{cm}^{-2}$, and the induced ^{156}Eu activity was observed for 29 days using a shielded 175 cm^3 HPGe detector.
The resulting γ–ray spectrum contained more than 200 lines, mainly from the remaining ^{152}Eu, ^{154}Eu activities and from natural background. From the observed ^{156}Eu transitions, 11 lines could be used for determining the induced activity. The resulting relative cross section for the quasi–stellar spectrum is

$$\frac{<\sigma(^{155}\mathrm{Eu})>}{<\sigma(^{197}\mathrm{Au})>} \quad = \quad 2.28 \pm 0.13,$$

corresponding to a Maxwellian averaged neutron capture cross section of the ^{155}Eu ground state

$$<\sigma(^{155}\mathrm{Eu})>_{30\,keV} \quad = \quad 1320 \pm 84\,mb.$$

The second radioactive isotope under investigation was ^{163}Ho. Under s–process conditions the terrestrially stable ^{163}Dy becomes unstable (*bound state decay*) giving rise to a branching of the synthesis path. The analysis of this branching allows to discuss the electron density in the stellar interior, since the half–lives of the involved isotopes depend strongly on this parameter.
The ^{163}Ho–sample ($t_{1/2} = 4570$ yr) was a fraction of a sample breeded in Los Alamos from enriched ^{162}Er, which had been chemically concentrated via the ion exchange technique by the ISOLDE group (Beyer and Ravn, 1984) This sample, which still contained some Er and Dy, was adsorbed on 5 mg graphite and then pressed to a pellet. The elemental composition was determined quantitatively using the X–ray fluorescence technique, and the isotopic composition was measured by mass spectroscopy, yielding a total of $N(^{163}\mathrm{Ho}) = (6.6 \pm 0.1) \cdot 10^{17}$ atoms.
In this case, six activations of 1 h duration were performed at the Van de Graaff accelerator (same method as the ^{155}Eu–measurement). The induced ^{164}Ho activity was counted with a 40 cm^3 HPGe–detector. The resulting stellar cross section is

$$<\sigma(^{163}\mathrm{Ho})>_{30keV} = 2125 \pm 95\,mb.$$

As a by–product of this activation, the stellar ^{162}Er cross section could be determined as well:

$$<\sigma(^{162}\mathrm{Er})>_{30keV} = 1624 \pm 124\,mb.$$

The analysis using the classical s–process approach and adopting the latest results on neutron density and temperature yields an allowed electron density range for the s–process between $1 \cdot 10^{27}$ and $3 \cdot 10^{27}$ cm^{-3}.

G.J. Beyer and H.L. Ravn 1984, private communications
W. Ratynski and F. Käppeler 1988, *Phys. Rev.C* **37**, 595

5. STELLAR (n,γ) CROSS SECTIONS OF THE GADOLINIUM ISOTOPES

K. Wisshak, K. Guber, F. Voß, F. Käppeler, L. Kazakov[1], N. Kornilov[1]

The (n,γ) cross sections of ^{152}Gd, ^{154}Gd, ^{155}Gd, ^{157}Gd, and ^{158}Gd have been measured with the same technique as used for the tin and barium isotopes discussed before. The main problem in these experiments is that the available enrichment for the rare s–only isotopes is rather low. This requires sizable corrections for isotopic impurities which caused significant systematic uncertainties in previous experiments. The good resolution in γ–ray energy of the Karlsruhe 4π BaF_2 detector allows for an efficient discrimination between capture events in different isotopes, resulting in smaller and more reliable corrections. Presently, most of the measurement is completed.

[1]IPPE Obninsk, Russia

INSTITUT FÜR KERNPHYSIK, ARBEITSGRUPPE STRAHLUNGSTRANSPORT, FORSCHUNGSZENTRUM JÜLICH GmbH

Systematics of Residual Mass Distributions of Accelerator Structure Materials

R. Baur, D. Filges and H. Schaal

Investigations for the simulations of residual mass distributions for accelerator structure materials at incident proton beam energies between 800 Mev and 3000 MeV were started in the frame of the feasibility study of the "European Spallation Source" (ESS) [1]. Residual mass distributions are important to study the induced radioactivity of accelerator structure material under certain beam loss conditions. For this purpose the HERMES [2] code system of KFA together with a decay data library ORIHET [3] were used. The residual mass distributions were simulated using the HETC/KFA-2 modul within the HERMES system. In Table 1 the relevant structure materials are given. In Figs. 2 and 3 some examples of residual mass distributions for the materials copper and niobium are shown.

REFERENCES

[1] H. Lengeler, Proposals for Spallation Sources in Europe, invited talk at EPAC, London 1994

[2] P. Cloth et al., KFA-Report Jül-2203 (1988)

[3] F. Atchison, private communication

Table 1. Relevant Accelerator Structure Materials

Target- Material	Incident Proton Energy [MeV]	Residual Nuclei Production per Source Proton
Al	800	0.4459
Al	1350	0.4121
Al	3000	0.3587
Al_2Mg_3	800	0.4674
Al_2Mg_3	1350	0.4685
Al_2Mg_3	3000	0.4554
Al_2O_3	800	0.4378
Al_2O_3	1350	0.4370
Al_2O_3	3000	0.4223
Steel (X 2 Cr Ni Mo 17 13 2)	800	0.5670
Steel (X 2 Cr Ni Mo 17 13 2)	1350	0.5684
Steel (X 2 Cr Ni Mo 17 13 2)	3000	0.5589
Cu	800	0.5818
Cu	1350	0.5841
Cu	3000	0.5430
Ni	800	0.5748
Ni	1350	0.5799
Ni	3000	0.5664
Nb	800	0.6258
Nb	1350	0.6225
Nb	3000	0.6152

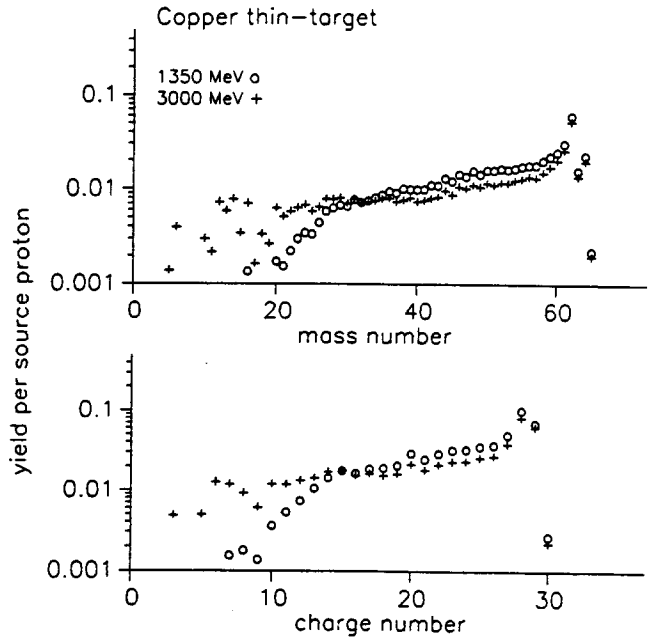

Fig. 1. Residual mass distribution for copper at 1350/3000 MeV incident proton beam as a function of mass number and charge number.

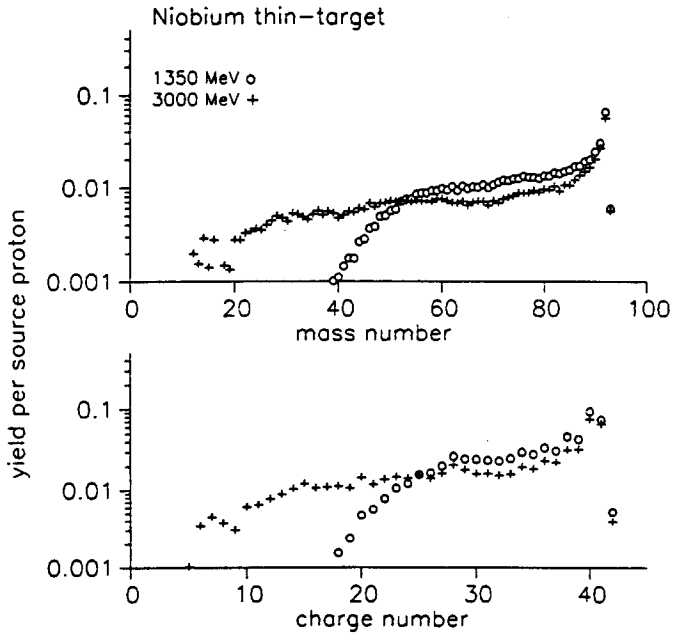

Fig. 2. Residual mass distribution for niobium at 1350/3000 MeV incident proton beam as a function of mass number and charge number.

INSTITUT FÜR NUKLEARCHEMIE
FORSCHUNGSZENTRUM JÜLICH

1. Complex Particle Emission Reactions

B. Neumaier, F. Rösch, S.M. Qaim, G. Stöcklin

In continuation of our fundamental studies on neutron and charged particle induced nuclear reactions involving complex particle emission [cf. 1,2 and previous Progress Reports] the $^{209}Bi(p,^{7}Be)^{203}Hg$ process was investigated radiochemically over the proton energy range of 20 to 70 MeV via identification of both the emitted particle (^{7}Be) and the product nucleus (^{203}Hg). Since the major part of ^{7}Be originated from interfering reactions on light mass impurity elements (C, N, O), the emphasis was placed on the study of the product nucleus ^{203}Hg. A clear evidence was obtained after thermochromatographic separation of radiomercury. The cross section data deduced are shown in Fig. 1. For proton energies up to 55 MeV the ^{203}Hg formation cross section is very low (74 - 224 nb) and refers to the real $(p,^{7}Be)$ reaction on ^{209}Bi. Above 55 MeV, however, the cross section increases rapidly, reaching a value of about 4 μb at 70 MeV. This is presumably due to the onset of the competing several nucleon (4p3n) emission process (for more details cf. [3]).

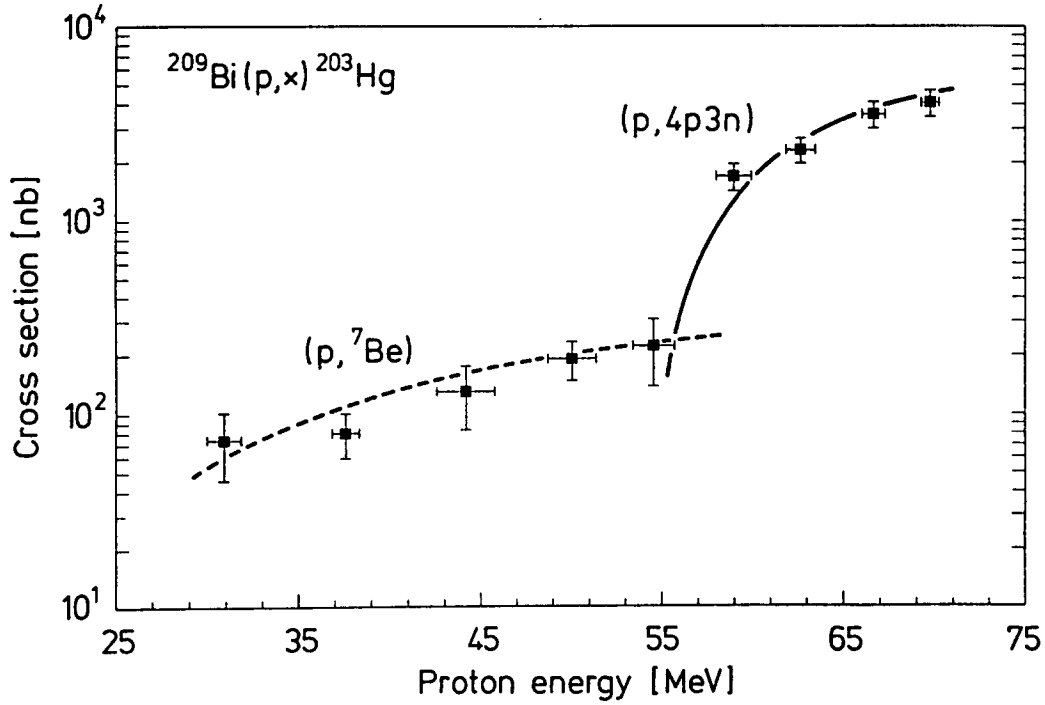

Fig. 1 Cross sections for the formation of ^{203}Hg in the interaction of ^{209}Bi with protons. The curves are eye-guides and are attributed to $(p,^{7}Be)$ and (p,4p3n) processes [cf. 3].

The (n,α) reaction at energies above 10 MeV is known to include significant contributions from direct processes. Whether the same applies to the (p,α) process is somewhat uncertain. We measured excitation functions of the $^{64}Ni(p,\alpha)^{61}Co$, $^{78}Kr(p,\alpha)^{75}Br$ and $^{86}Sr(p,\alpha)^{83}Rb$ processes from the respective thresholds to 18 MeV. The results for the $^{78}Kr(p,\alpha)^{75}Br$ reaction have already been published [4], those for the other target nuclei are new. In each case highly enriched target material was used. Statistical model calculations incorporating precompound as well as direct effects were performed in collaboration with the IRK, Vienna (M. Uhl). In general, the contribution of direct processes to α-emission in proton induced reactions appears to be governed by Q-value effects: for target nuclei with high (p,n) Q-values, the direct contribution to α-emission is relatively small.

2. Isomeric Cross Section Ratios

F.-O. Denzler, M. Faßbender, A. Fessler, S. Sudár, F. Rösch, S.M. Qaim

Continuing our studies on isomeric cross section ratios [cf. 5,6] we investigated the following isomeric pairs:

a) $^{93m,g}Tc$, $^{94m,g}Tc$ and $^{95m,g}Tc$ in (^{3}He,xn)-reactions on ^{93}Nb over the energy range of 10 to 35 MeV. The isomeric pair $^{94m,g}Tc$ was also investigated in the $^{92}Mo(\alpha,pn)$-process for energies up to 26 MeV. Nuclear model calculations are in progress in collaboration with the IRK, Vienna (B. Strohmeier).

b) $^{52m,g}Fe$ and $^{53m,g}Fe$ in (^{3}He,xn)-reactions on ^{52}Cr over the energy range of 10 to 35 MeV. A rapid radiochemical separation of the short-lived ^{52m}Fe ($T_{1/2}$ = 46s) was developed. Both ^{53m}Fe and ^{52m}Fe have relatively high spins and are interesting cases for study. The isomeric state ^{52m}Fe was previously observed only in heavy ion reactions. The measured isomer ratios were interpreted so far only qualitatively.

c) Experimental studies on the isomeric pair $^{58m,g}Co$ formed in several nuclear reactions (cf. last Progress Report) were completed in collaboration with the Kossuth University, Debrecen, Hungary. Nuclear model calculations using the code STAPRE were performed. The experimental and theoretical results for the $^{61}Ni(p,\alpha)^{58m,g}Co$ process are shown in Fig. 2. The yield of the high spin isomer increases with the increasing projectile energy. The experimental and theoretical data agree for energies up to 10 MeV but at higher energies the model calculation gives consistently lower values [5]. The spin distribution of the level density (characterized by η) has some influence at energies above 10 MeV [5].

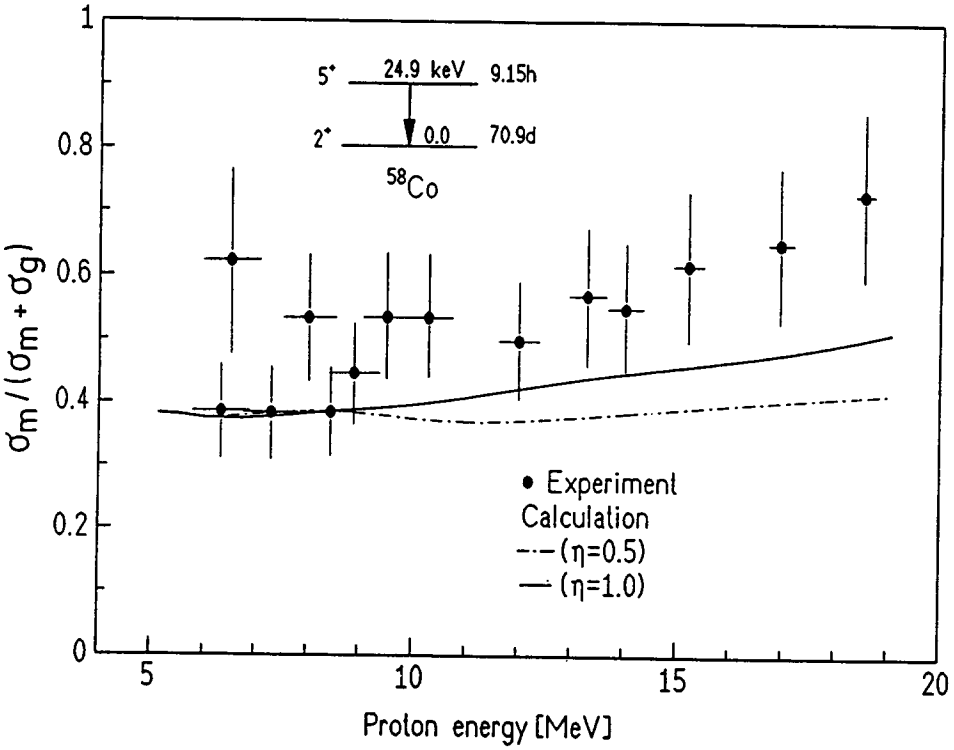

Fig. 2 Isomeric cross section ratio for the isomeric pair $^{58m,g}Co$ formed via $^{61}Ni(p,\alpha)$-reaction, plotted as a function of incident proton energy [cf. 5].

In addition to the experimental and theoretical work on isomeric cross section ratios described above, a brief survey of the recent developments in this field of study was performed and the areas needing further attention were outlined [cf. 7].

3. Fast Neutron Induced Reaction Cross Sections

R. Klopries, S.M. Qaim

(Relevant to request identification numbers: 861026 R, 861027 R)

Excitation functions were measured for the reactions $^{89}Y(n,2n)^{88}Y$, $^{89}Y(n,p)^{89}Sr$ and $^{89}Y(n,\alpha)^{86}Rb$ from the respective thresholds to 13.3 MeV neutron energy. The reaction products ^{89}Sr ($T_{1/2}$ = 50.5 d) and ^{86}Rb ($T_{1/2}$ = 18.7 d) decay primarily by β^- emission. A radiochemical separation of each product from the bulk Y_2O_3 target material was mandatory. The radioactivity was determined via low-level β^- counting. The cross sections for the (n,2n) reaction agree with the literature data. For the (n,p) and (n,α) reactions the cross sections lie in the mb region. The present measurements describe the first systematic study on the (n,p) and (n,α) reactions on ^{89}Y in the energy region between 8 and 13 MeV. The results show the same trends as reported by us for target nuclei with A = 60 to 80 [cf. 6,8].

4. Activation Cross Section Data Relevant to Proton Therapy

B. Scholten, M. Faßbender, S.M. Qaim, G. Stöcklin

The Research Centre Jülich is planning a proton therapy unit at the newly commissioned facility "Cooler Synchrotron" (COSY). There is some interest in measuring cross sections of nuclear reactions induced by 50 to 250 MeV protons on materials of biological interest. Both long-lived activation products (^{7}Be, ^{3}H, ^{22}Na, etc.) and short-lived β^+ emitting radioisotopes (^{11}C, ^{14}O, ^{15}O, ^{18}F, etc.) need to be studied, the latter in connection with the dose verification via Positron Emission Tomography (PET) after the proton therapy. We started measurements on the excitation function of the (p,^{7}Be) reaction on C, N, O, Si and Fe in the proton energy range of 100 to 180 MeV since the available data base in this energy region is rather weak. Irradiations were done at the Svedberg Laboratory Uppsala and the subsequent radiochemical work and activity measurement at Jülich. The data processing is in progress. Some preliminary studies on the formation of ^{11}C and ^{18}F in 72 MeV proton induced reactions on C and O were performed using the irradiation facility at PSI Zürich.

5. Excitation Functions Relevant to Radioisotope Production

F.-O. Denzler, M. Faßbender, A. Fessler, Z.B. Alfassi, Z. Kovács, F. Tárkányi, B. Scholten, F. Rösch, S.M. Qaim, G. Stöcklin

In continuation of our studies [cf. 4, 9, 10] on the production of medically important short-lived radioisotopes we measured excitation functions of several nuclear reactions relevant to the production of the β^+ emitting radioisotopes ^{52}Fe, ^{94m}Tc and ^{124}I.

^{52}Fe ($T_{1/2}$ = 8.27 h) is a useful radionuclide for studying the biochemistry of iron based compounds with potential applications in nuclear medicine, particularly in red blood cell studies. It is commonly produced via the ^{55}Mn(p,4n)^{52}Fe reaction using ≈ 70 MeV protons. The ^{52}Cr(^{3}He,3n)^{52}Fe process appeared to be suitable for production at a compact cyclotron. The nuclear data available in the literature for this reaction are, however, scanty. Furthermore, the β^+ emitting radioisotope ^{53}Fe ($T_{1/2}$ = 8.5 min) could be a possible substitute for ^{52}Fe, especially for applications where its short half-life is not a disadvantage. No measurements have been reported hitherto on the ^{52}Cr(^{3}He,2n)^{53}Fe reaction. We measured excitation functions of the two processes, viz. (^{3}He,2n) and (^{3}He,3n), and the results are reproduced in Fig. 3. The optimum ^{3}He-energy ranges for the production of ^{52}Fe and ^{53}Fe were found to be $E_{^{3}He}$ = 36 → 17 MeV and $E_{^{3}He}$ = 17 → 7 MeV, respectively, with the expected thick

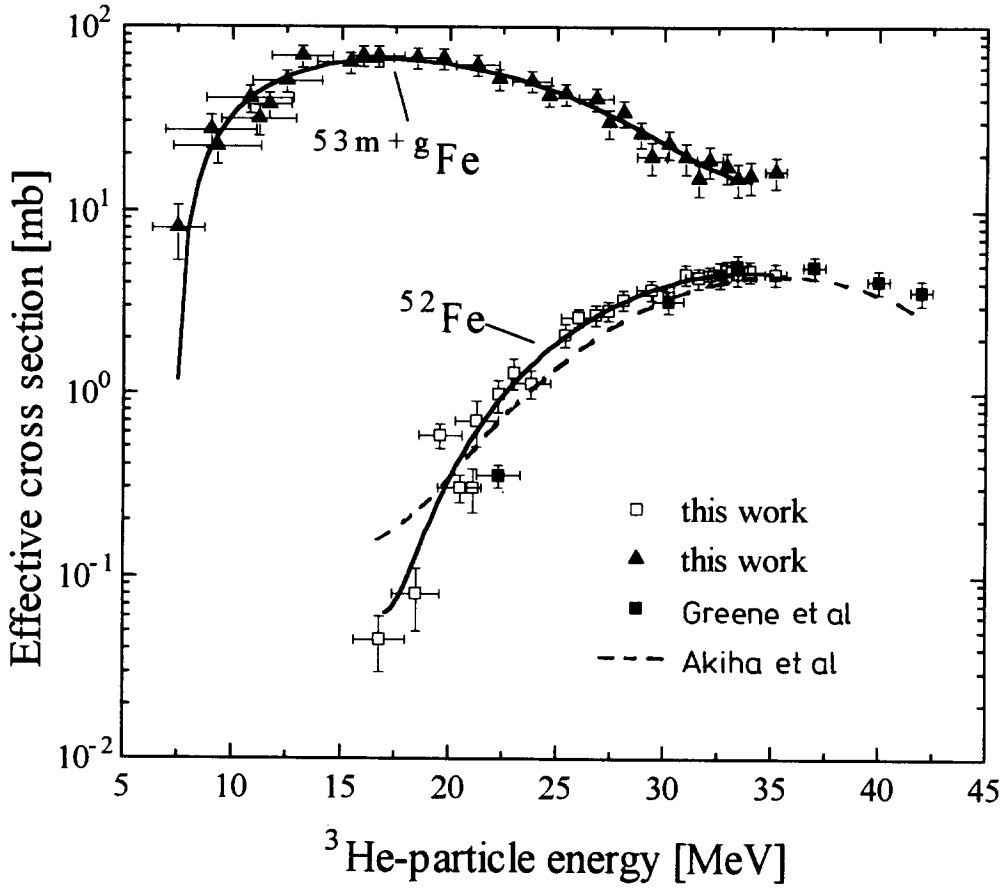

Fig. 3 Excitation functions of ^{nat}Cr(^{3}He,xn)-processes leading to the formation of ^{52}Fe and $^{53m+g}$Fe. The cross sections are given as effective cross sections, i.e. assuming ^{nat}Cr to be a single isotope [cf. 11]. The literature data for ^{52}Fe (Greene et al., IJARI *21*, 719 (1970) and Akiha et al., Radiochimica Acta *18*, 108 (1972)) are also shown.

target yields of 1.3 MBq (35 μCi)/μAh for ^{52}Fe and 78 MBq (2.1 mCi)/μAh for ^{53}Fe. Due to the low yields of the (^{3}He,3n) process, the radioisotope ^{52}Fe can thus be produced only in limited amounts. The yield of ^{53}Fe is high; however, the time needed for chemical processing is rather long. The quantity available at End of Separation (EOS) is rather low for medical application (for more details cf. [11]).

The β^{+} emitting radioisotope ^{94m}Tc ($T_{1/2}$ = 52 min) is a potentially useful radioisotope for quantifying biodistribution of Tc-radiopharmaceuticals in humans via PET. It can be produced via several nuclear reactions. The cross section data for the ^{94}Mo(p,n)^{94m}Tc reaction were measured using 94% enriched ^{94}Mo and were reported in the last Progress Report. Excitation functions were now measured for the ^{93}Nb(^{3}He,2n)^{94m,g}Tc and other competing processes in the energy range of 10 to 35

MeV. Similarly α-particle induced reactions on 97% enriched ^{92}Mo were investigated radiochemically, with special respect to the formation of ^{94m}Tc. Two nuclear processes, namely ^{92}Mo(α,pn)^{94m}Tc and ^{92}Mo(α,2n)^{94}Ru $\xrightarrow[52\,\text{min}]{EC,\beta^+}$ ^{94m}Tc, contribute to the formation of ^{94m}Tc. A comparison of the various investigated production routes is given in Table 1. Evidently the ^{94}Mo(p,n)-process gives the highest ^{94m}Tc yield and low impurity (≈ 6% ^{94g}Tc). On the other hand, the ^{92}Mo(α,2n)^{94}Ru $\xrightarrow[52\,\text{min}]{EC,\beta^+}$ ^{94m}Tc route is also interesting since ^{94}Ru decays almost exclusively to ^{94m}Tc and no ^{94g}Tc is formed as impurity. Nonetheless, the ^{94}Mo(p,n)-process is the method of choice since it can be used even at a small cyclotron.

Table 1. Comparison of production routes for ^{94m}Tc

Route	Optimum energy range [MeV]	Amount of ^{94g}Tc in ^{94m}Tc at EOB (%)	Other technetium radioisotopes at EOB [%]	Calculated thick target yield of ^{94m}Tc MBq/μAh	
				EOB	EOB + 90 min
^{94}Mo(p,n)^{94m,g}Tc	13 → 7	6	^{93m,g}Tc: 1	2000	588
^{93}Nb(^{3}He,2n)^{94m,g}Tc	18 → 10	> 25	^{93m,g}Tc: 5 ^{95}Tc: < 1	34	10
^{92}Mo(α,pn)^{94m,g}Tc	26* → 18	> 30	^{95m,g}Tc: 1	98	29
^{92}Mo(α,2n)^{94}Ru → ^{94m}Tc	26* → 18	< 1	^{95g}Tc: 7 (EOB + 90 min)		34

* Maximum energy available at CV 28 (not optimum).

The radioisotope ^{124}I ($T_{1/2}$ = 4.15 d) is the only longer-lived β^+ emitting isotope of iodine and has found application in labelling some biomolecules, specific in tumour research with PET. For production at a small cyclotron the ^{124}Te(p,n)^{124}I reaction could be used. The excitation function is not known well. We performed detailed measurements from threshold to 21 MeV using thin samples which were prepared via electrolytic deposition of 99.9% enriched ^{124}Te on Ti-backing.

The results are shown in Fig. 4 together with the literature data. The cross sections at the maxima of the literature and our curves appear to agree within the limits of experimental errors. There is, however, an energy shift of about 2.5 MeV in our data. Since our measurements were done using three primary proton energies (21,17 and 12 MeV) which have been recently characterized by a time of flight method, we

believe our data to be more accurate. Evidently, the ^{124}Te(p,n)-process is a suitable reaction for production of ^{124}I.

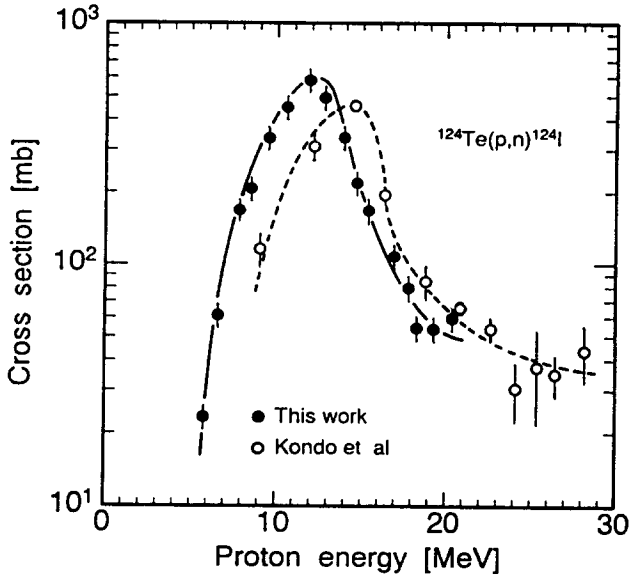

Fig. 4 Excitation function of the ^{124}Te(p,n)^{124}I process. The literature data (Kondo et al., IJARI *28*, 395 (1977)) are also shown.

References

[1] B. Scholten, S.M. Qaim, G. Stöcklin: A systematic study of (n,^{7}Be) reactions on medium and heavy mass nuclei induced by 53 MeV d(Be)-breakup neutrons, Radiochimica Acta 62 (1993) 107

[2] B. Scholten, S.M. Qaim, G. Stöcklin: Radiochemical studies of proton induced ^{7}Be-emission reactions in the energy range of 40 to 100 MeV, Radiochimica Acta, in press

[3] B. Neumaier, F. Rösch, S.M. Qaim, G. Stöcklin: Radiochemical study of the ^{209}Bi(p,^{7}Be)^{203}Hg-process from 20 to 70 MeV via identification of the emitted particle (^{7}Be) and the product nucleus (^{203}Hg), Radiochimica Acta, in press

[4] F. Tárkányi, Z. Kovács, S.M. Qaim: Excitation functions of proton induced nuclear reactions on highly enriched ^{78}Kr: relevance to the production of ^{75}Br and ^{77}Br at a small cyclotron, Appl. Radiat. Isot. 44 (1993) 1105

[5] S. Sudár, F. Szelecsényi, S.M. Qaim: Excitation function and isomeric cross section ratio for the $^{61}Ni(p,\alpha)^{58m,g}Co$ process, Phys. Rev. C48 (1993) 3115

[6] F. Cserpák, S. Sudár, J. Csikai, S.M. Qaim: Excitation functions and isomeric cross section ratios of the $^{63}Cu(n,\alpha)^{60m,g}Co$, $^{65}Cu(n,\alpha)^{62m,g}Co$ and $^{60}Ni(n,p)^{60m,g}Co$ processes from 6 to 15 MeV, Phys. Rev. C49 (1994) 1525

[7] S.M. Qaim: Recent developments in the study of isomeric cross sections (Invited Paper), Proc. Int. Conf. on Nuclear Data for Science and Technology, Gatlinburg, May 1994, in press

[8] M. Bostan, S.M. Qaim: Excitation functions of threshold reactions on ^{45}Sc and ^{55}Mn induced by 6 to 13 MeV neutrons, Phys. Rev. C49 (1994) 266

[9] S.M. Qaim, G. Stöcklin: Excitation functions of $^{74}Se(d,xn)^{75,74m}Br$ reactions: comparative evaluation of possible routes for the production of ^{75}Br at a small cyclotron, Appl. Radiat. Isot. 44 (1993), 1443

[10] F. Rösch, S.M. Qaim: Nuclear data relevant to the production of the positron emitting technetium isotope ^{94m}Tc via the $^{94}Mo(p,n)$-reaction, Radiochimica Acta 62 (1993) 115

[11] A. Fessler, Z.B. Alfassi, S.M. Qaim: Excitation functions of ^{3}He-particle induced nuclear reactions on natural chromium: possibilities of production of ^{52}Fe, ^{53}Fe and ^{52}Mn for medical use, Radiochimica Acta, in press

INSTITUT FÜR KERN-UND TEILCHENPHYSIK TECHNISCHE UNIVERSITÄT DRESDEN

1. Fragment-Neutron and Neutron-Neutron Correlations in ^{252}Cf spontaneous-fission +

I. DÜRING, U. JAHNKE[1)], H. MÄRTEN[2)]
[1)] HMI Berlin, [2)] now at IRMM Geel (Belgium)

The combination of a twin ionization chamber with a 2x2π-Gd-loaded scintillator tank [1] was used for the high-precision, exclusive measurement of the multi-fold fission distribution in relevant fragment, neutron, and γ-ray co-ordinates. Various correlations were studied and related to mass asymmetry (A_l/A_h), elongation (total kinetic energy TKE of fragments) as well as shape-asymmetry (neutron number ratio ν_l/ν_h) of the scission configuration. A comprehensive theoretical interpretation of the results was performed within an energy-conservation-consistent scission point model including temperature-dependent shell and pairing effects SCISSY [2] as well as on the basis of its modifications: (i) pure liquid-drop model SC-LDM (neclecting the microscopic corrections), (ii) deformation energy description assuming average nuclear stiffnessrelated to spherical shells SC-STIFF. All approaches were combined with a full-scale statistical model of neutron emission.
The experimental mass yields for fixed shape-asymmetry ν_l/ν_h (cf. examples in Fig. 1) indicate cold compact (0/0), cold deformed (5/5), and cold shape-asymmetric (2/6) fission by odd-even effects mainly due to proton pairing. The two-dimensional distribution $P(\nu_l, \nu_h)$ as represented in Fig. 2 for the fragmentation 120/132 can be understood as a qualitative indication of the potential energy surface at scission depending on the typical individual deformations of the complementary fragments. The ratio of the neutron-multiplicities as a function of TKE for given mass-asymmetry (Fig. 3) is nearly constant and corresponds to the results of SC-STIFF. It is shown that the (dynamically caused) statistical averaging of microscopic effects is dominant in the fission process (even at large elongations in contrast to the original scission point model). The measured covariances of neutron multiplicities ($cov = \sum_{\nu_l} \sum_{\nu_h} P(\nu_l, \nu_h)(\nu_l - \bar{\nu_l})(\nu_h - \bar{\nu_h})$) as function of mass and TKE shown in Fig. 4 were found to be in good agreement with theoretical results. This confirms the model assumption concerning the energy balance at scission and the statistical independence of the neutron emission cascades.

References

[1] I. Düring, A.Ruben, M. Adler, H. Märten, B. Cramer, U. Jahnke, Proceedings "Workshop on High-Resolution Spectroscopy of Fission Fragments, Neutrons and γ-Rays", Dresden 1.-2. Febr. 1993, Editors: H.Märten and K.D. Schilling, FZR 93-08(1993)104

[2] H. Märten, Proc. Seminar on Fission Pont d'Oye II, 1991 Oct. 23.-25., ed. C. Wagemans, p. 15

+ Supported by BMFT under contract 06 DD 112

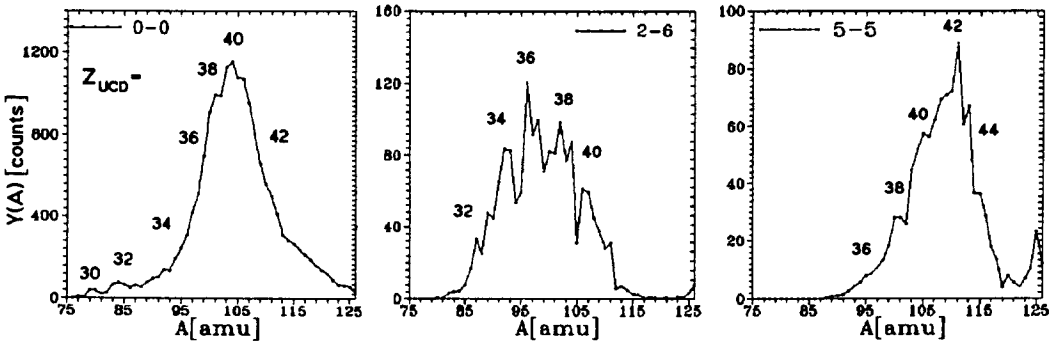

Fig. 1: Fragment mass yield for fixed ν_l/ν_h. The data structures are compared with the position of even Z according to unchanched charge distribution UCD.

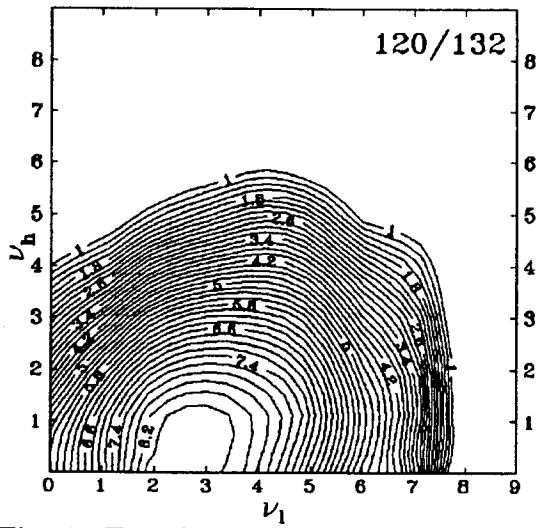

Fig. 2: Two-dimensional neutron multiplicity distribution for the fragmentation 120/132.

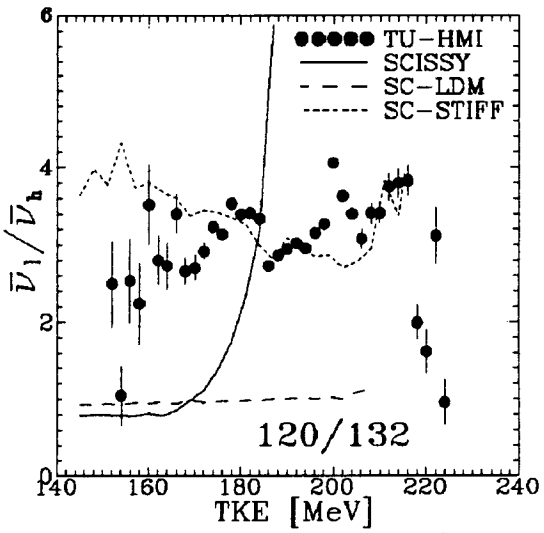

Fig. 3: Ratio of neutron multiplicity as function of TKE for the fragmentation 120/132.

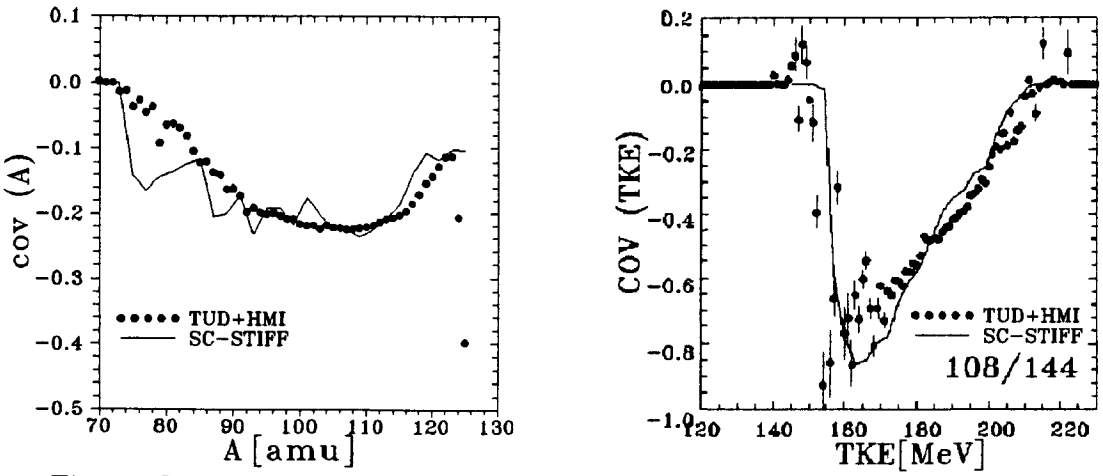

Fig. 4: Covariance of neutron multiplicity as a function of mass and TKE.

2. Benchmarks of Iron Nuclear Data

H. Freiesleben, W. Hansen, D. Richter, K. Seidel, S. Unholzer

One of the main objects in the field of neutronics for TOKAMAK based fusion reactors as NET/ITER is the efficient shielding of the superconducting magnets from neutrons and γ-rays. The fluence of fast neutrons in the magnet coils, the number of atomic displacements in their copper stabilizer and the nuclear heating in the winding pack are parameters of the ITER shield design which are deduced from the neutron and photon fluxes (Φ_n and $\Phi\gamma$) penetrating the shield [1]. The main deficiencies of calculated shield parameters stem from the evaluated nuclear data used, and there the greatest contibutions arise from iron data [2]. Therefore, iron slabs (1x1 m^2 and a thickness of 30 cm) were irradiated with 14 MeV neutrons and the Φ_n and Φ_γ penetrating the assembly were determined. Because gaps, such as between two adjacent blanket segments, are a special aspect of radiation shields (e.g. streaming by forward-peaked nuclear processes), the investigations have been extended to the inclusion of vertical gaps in the slab (gap width 1 cm or 5 cm) at distances of 10 cm or 20 cm from the slab centre. The arrangement is outlined in Fig. 1.

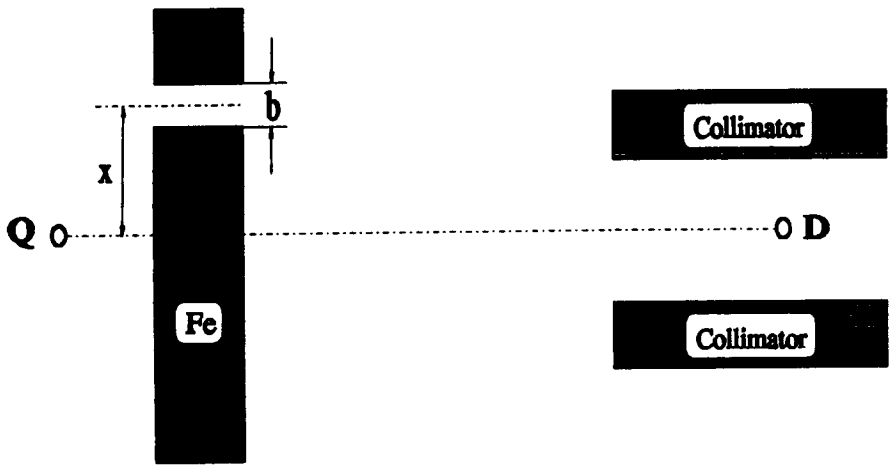

Fig. 1: Horizontal cross section of the benchmark geometry
(Q - neutron source; D - detector; distance QD = 349 cm; x,b - position and width of vertical gap)

As described in the previous progress report differential energy flux spectra as well as time-of-arrival fluxes for neutrons and photons were determined in two-dimensional measurements. This method allows simultaneous recordings of pulse height and time spectra in the energy range 1 ... 14 MeV for neutrons and between 160 keV and 10 MeV for photons. $\Phi_n(t)$ is used as additional check of the neutron nuclear data, whereas $\Phi_\gamma(t)$ is needed for the discrimination of photons produced by neutrons in walls and floor of the experimental hall, in the

detector, and in its collimator.
In the low-energy range (30 keV ... 3 MeV) neutron flux spectra were measured by use of proton recoil counter and stilbene scintillation spectrometers.
Absolutely calibrated detectors [3,4,5] and the source strength monitoring allow to measure on an absolute scale.
For the calculations of the benchmark the 3-dimensional Monte-Carlo-code MCNP [6] version 3B, that is coupled neutron-photon-transport, is used. As in the experiment the events are acquired two-dimensionally as N(E,t). Collimator, floor, walls, target backing, air, assembly rack etc. are taken into account, so that the calculated Φ can be directly compared with the measured one. The data base is EFF-1, the European Fusion File version 1 [7].

2.1. Neutron Flux Spectra in the Resonance Energy Region

The measured neutron spectrum from the solid slab is compared in Fig. 2a with the calculated distribution. The agreement is satisfying between about 0.2 MeV and 3 MeV. A significant excess of neutrons is observed below 0.2 MeV.

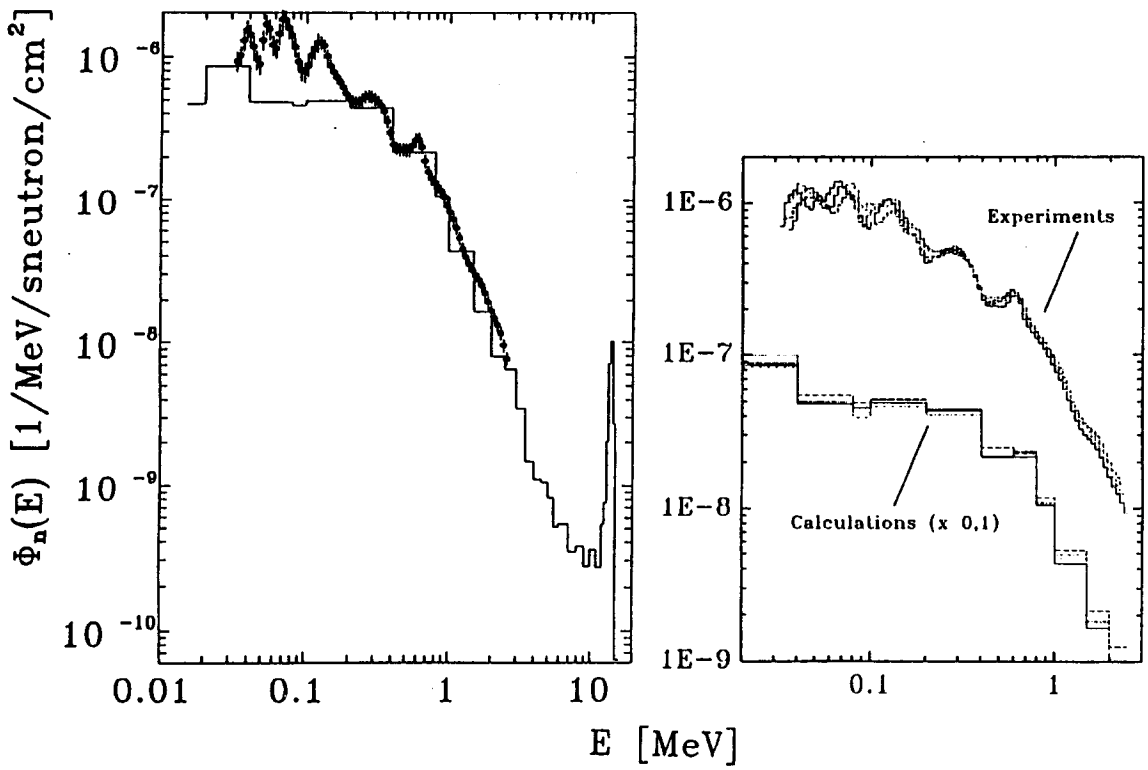

Fig. 2a: Low-energy part of the neutron flux spectrum from the solid slab normalized to one source neutron (* experiment, — calculation)

Fig. 2b: Neutron flux spectra from the solid slab (—) and from the assemblies with a gap x=10cm, b=5cm (- - -); x=10cm, b=1cm (···); x=20cm, b=5cm (—·—) normalized to one source neutron

This behaviour is also observed in all measurements with a gap in the assembly as shown in Fig. 2b. Position and width of gaps do not change the spectrum significantly in this energy range. The independently measured spectra on the one hand and the calculations on the other hand have the same shape with only small differences. Consequently, the origin of the underestimation of neutrons in the range below 200 keV should be in the nuclear data. A larger cross section in the region of fluctuating, overlapping resonances [8] could lead to an enhanced transport of neutrons in the region where the surplus is measured.

2.2 Pre-compound Processes and Neutron Flux

Experimental energy spectra of the neutron flux are compared with the corresponding calculated distributions in Fig. 3 for the energy region where pre-compound neutron emissions may have influence. A significant surplus of neutrons is observed for 5 MeV < E < 13 MeV in both cases, the solid Fe slab and the assembly with gap.
A comparison of Fig. 3a and Fig. 3b shows that the measured neutron flux in this energy range is about 1.5 times greater from the assembly with gap than from the solid Fe block. The ratio of the calculated values is also about 1.5. Therefore, the origin of the experimental neutron excess should be the same in first order.

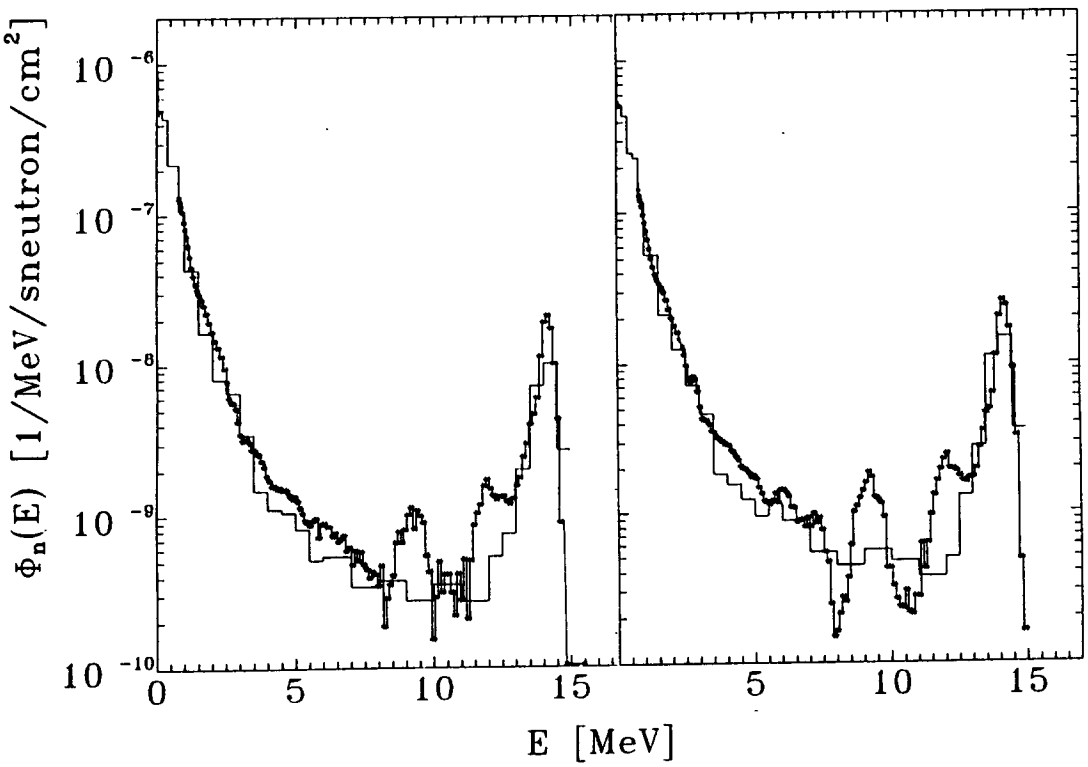

Fig. 3: High- energy part of the neutron flux spectrum from the solid slab (3a. left hand) and from the assembly with gap x=10cm and b=5cm (3b. right hand) normalized to one source neutron (* experiment, — calculation)

The independently determined time-of-arrival spectra of the neutron flux have experimental to calculated ratios significantly greater 1.0 for 80 ns < t < 130 ns as shown in Fig. 4 for the solid Fe slab. That is just the time range where most of the neutrons with energies between about 10 MeV and 5 MeV arrive.

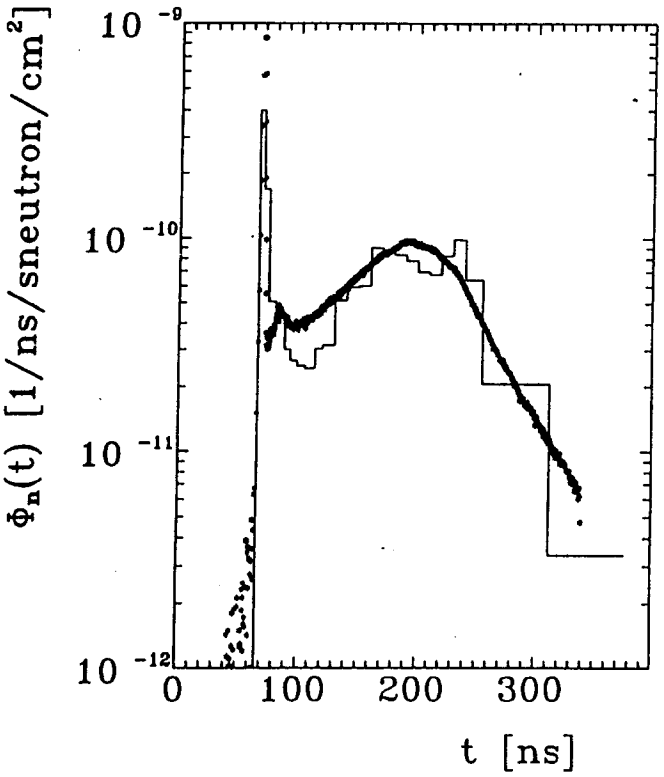

Fig. 4: Time-of-arrival spectrum of the neutron flux from the solid slab normalized to one source neutron
(* experiment, — calculation)

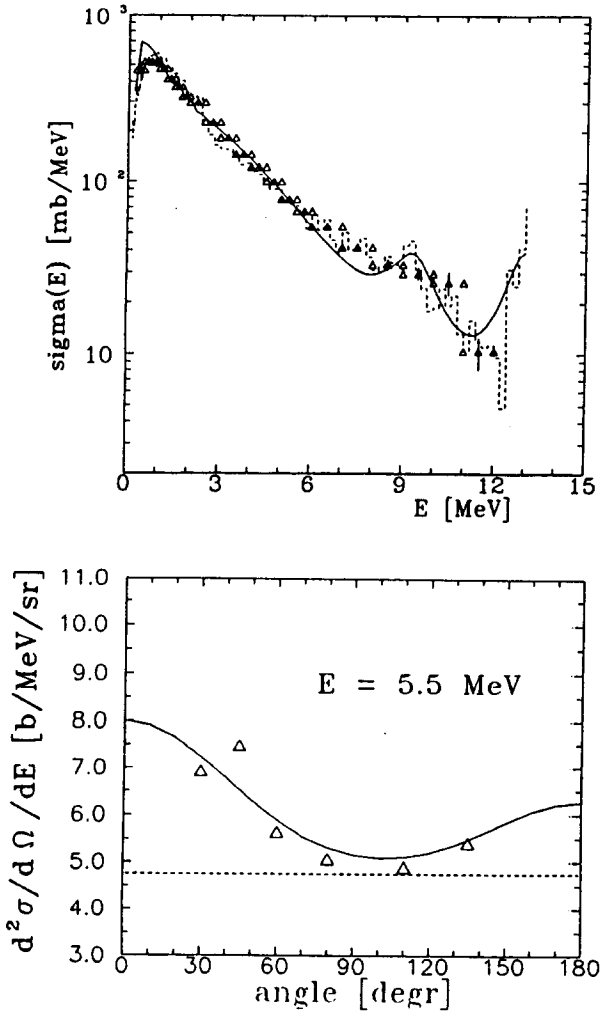

Fig. 5: Neutron emission cross section from Fe at 14 MeV incidence energy, angle-integrated (5a. upper part) and double differential at 5.5 MeV emission energy (5b. lower part) as used in the EFF-1 library (- - -), evaluated from experimental data (ΔΔΔ [9]) measured (Δ [10]), and calculated with a SMD / SMC model (— [11])

This discrepancy between calculated and experimental results can be discussed in connection with the neutron emission cross section at 14 MeV neutron incidence energy. The angle-integrated energy spectrum of the EFF-1 library cross section is compared in Fig. 5a with evaluated experimental data [9] and with a theoretical calculation based on multistep-direct and multistep-compound mechanisms [10]. The agreement is satisfying. But, differences

appear in the angular distributions of the emitted neutrons, as shown in Fig. 5b for E = 5.5 MeV. Isotropic emission is assumed for the library data up to about E = 13 MeV, whereas pre-compound processes (multistep-direct in the model) that are dominating in this region, are forward-peaked. In the benchmark those neutrons are observed which are emitted around 0° and have (single-scattered) a maximum angle of 60°.

2.3 Photons Produced by Neutrons

Experimental spectra of the photon flux are compared in Fig. 6 with the corresponding calculated distributions. The γ-rays from the de-excitation of the first ^{56}Fe level at E = 0.85 MeV and from higher levels have about 40% greater intensity than predicted, for both the solid and the gap assembly. The flux from the solid block is about 70% of those from the same assembly but with gap inserted. The peak at 0.51 MeV contains a remarkable contribution of photons from the annihilation of pair-production positrons.
For a discussion of the results it must be taken into consideration that the photons observed originate from relatively small depth in the Fe at the detector side of the assembly (e.g. 80% of all photons come from a slab of 5 cm thickness). Therefore, the gap enhances the photon flux significantly, and this "geometry" effect is described by the 3D-code. But, the library data underestimate the forward-peaking of the neutron transport as shown in 2.2, leading to smaller photon production rates at the detector side of the slabs in the calculations.

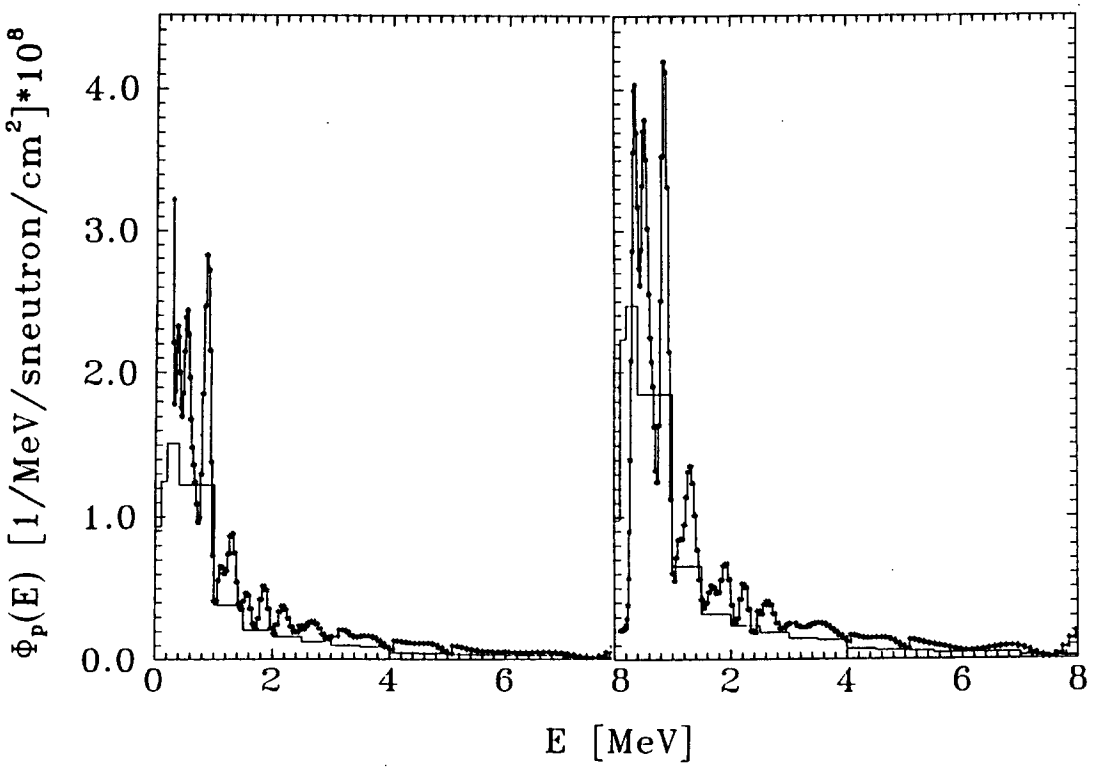

Fig. 6: Photon flux spectrum from the solid slab (6a. left hand) and from the assembly with gap x=20cm and b=5cm (6b. right hand) normalized to one source neutron (* experiment, — calculation)

References

[1] W. Daenner. ITER Expert Meeting on Shielding Experiments and Analysis. Garching (FRG), Febr. 12 - 14, 1990. ITER-IL-5-0-5 (1990).

[2] A. Santamarina and T. Parish. Sensitivity and uncertainty analysis of the NET magnet neutronic design parameters to uncertainties in cross section data. CEA 917/333 (1991).

[3] M. Tichy, H. Klein and J. Pulpan. Calibration of an NE-213 scintillator. Report PTB-7.2-92-1 (1992).

[4] H. Klein, A. Novotny, M. Tichy, S. Unholzer. Photon Response of a NE-213 Detector. PTB Braunschweig. unpublished

[5] D. Albert, et al.. Die elektronische Apparatur des Rossendorfer Rückstoßperotonen-Proportional-zählrohr-Spektrometers. Kernenergie 21(1978)82.

[6] J. F. Briesmeister. MCNP - A general Monte Carlo code for neutron and photon transport. LA-7396. Los Alamos N. L. (1986).

[7] H. Gruppelaar. Processing of the EFF-1 and EFF-2 data files. EFF-Doc-46

[8] F.H. Fröhner. Cross Section Fluctuation Factors for Natural Iron. Progress Report on Nucl. Data Research in the Federal Republic of Germany. NEA/NSC/DOC(93)17, INDC(Ger)-037/LN, Jül-2803, July 1993

[9] A. Pavlik and H. Vonach. Evaluation of the angle integrated neutron emission cross sections from the interaction of 14 MeV neutrons with medium and heavy nuclei. Physics Data 13-4 (1988).

[10] A. Takahashi, et al.. Double and single differential neutron emission cross sections at 14.1 MeV. Oktavian Report A-92-01. Osaka University (1992).

[11] H. Kalka. A model for statistical multistep reactions. INDC(GDR)-060/L. IAEA, Vienna (1990).

3. Evaluated L X-Ray Transition Energies

T.Reiche, G.Zschornack

The steadily increasing interest in atomic data is motivated by various applications of XRF and accelerator-based PIXE and HIXE. Demanded are precision data from neutral free atoms and from chemical compounds.

An evaluation of X-ray transition energies of the K-series was presented in an earlier work [1]. In addition transitions of the L X-ray series for all atomic numbers were analyzed. Results of the investigation of L_{α_1} transitions are presented in Fig.1. In comparison to the experimental results of Bearden [2] certain experimental transition energies from different authors (Cauchois et al. [3], Maria et al. [4], Mooney et al. [5], Ohno [6]) are shown. Further more, theoretical values of Huang et al. [7] were compared with experimental results of Bearden [2] and theoretical data of Uchai et al. [8].

On the left side of Fig.1 deviations of measured X-ray energies are presented in comparison to the values of Bearden [2]. While the majority of the data is consistent within $\Delta E/E < 1 \cdot 10^{-4}$, in some cases deviations appear in the per thousand region. Among others this is found for individual elements due to the measuring problems and difficulties in the handling of corresponding probes.

On the right side of Fig.1 deviations of measured L_{α_1} X-ray transition energies [2] and of theoretical values from Uchai [8] in comparison to theoretical results of Huang et al. [7] are shown. The experimental values show a certain systematics in their deviations over the whole Periodic System according to the values of Huang, i.e. the theory reproduces experimental results with a precision of about $\Delta E/E \approx 10^{-4}$. This fact also counts for the comparison between the works of Huang and Uchai, whereby the confidence limits of usual determination methods are confirmed.

This work has been supported by the BMFT under contract No. 06 DD 111.

References

[1] S.Fritzsche, A.M.M.Mohammedein, G.Musiol, I.Reiche, F.Schubert, G.Zschornack; Nucl. Instr. Methods, B50 (1990) 353

[2] J.A.Bearden; Review of Modern Physics, 39 (1967) 7

[3] Y.Cauchois, C.Senemaud; Wavelengths of X-ray emission lines and absorption edges, Int. Tables of Selected Constants, 18 (1978)

[4] H.Maria, J.Dalmasso; X-Ray Spectrometry, 11 (1982) 79

[5] T.Mooney, E.Lindroth, P.Indelicato, E.G.Kessler Jr., R.D.Deslattes; Physical Review, A45 (1992) 1531

[6] M.Ohno, R.E.LaVilla; Physical Review, A45 (1992) 4713

[7] K.N. Huang, M.Aoyagi, M.S.Chen, B.Crasemann, H.Mark; Atomic Data and Nuclear Data Tables, 18 (1976) 243

[8] W.Uchai, C.W.Nestor Jr., S.Raman, C.R.Vane; Atomic Data and Nuclear Data Tables, 34 (1986) 201

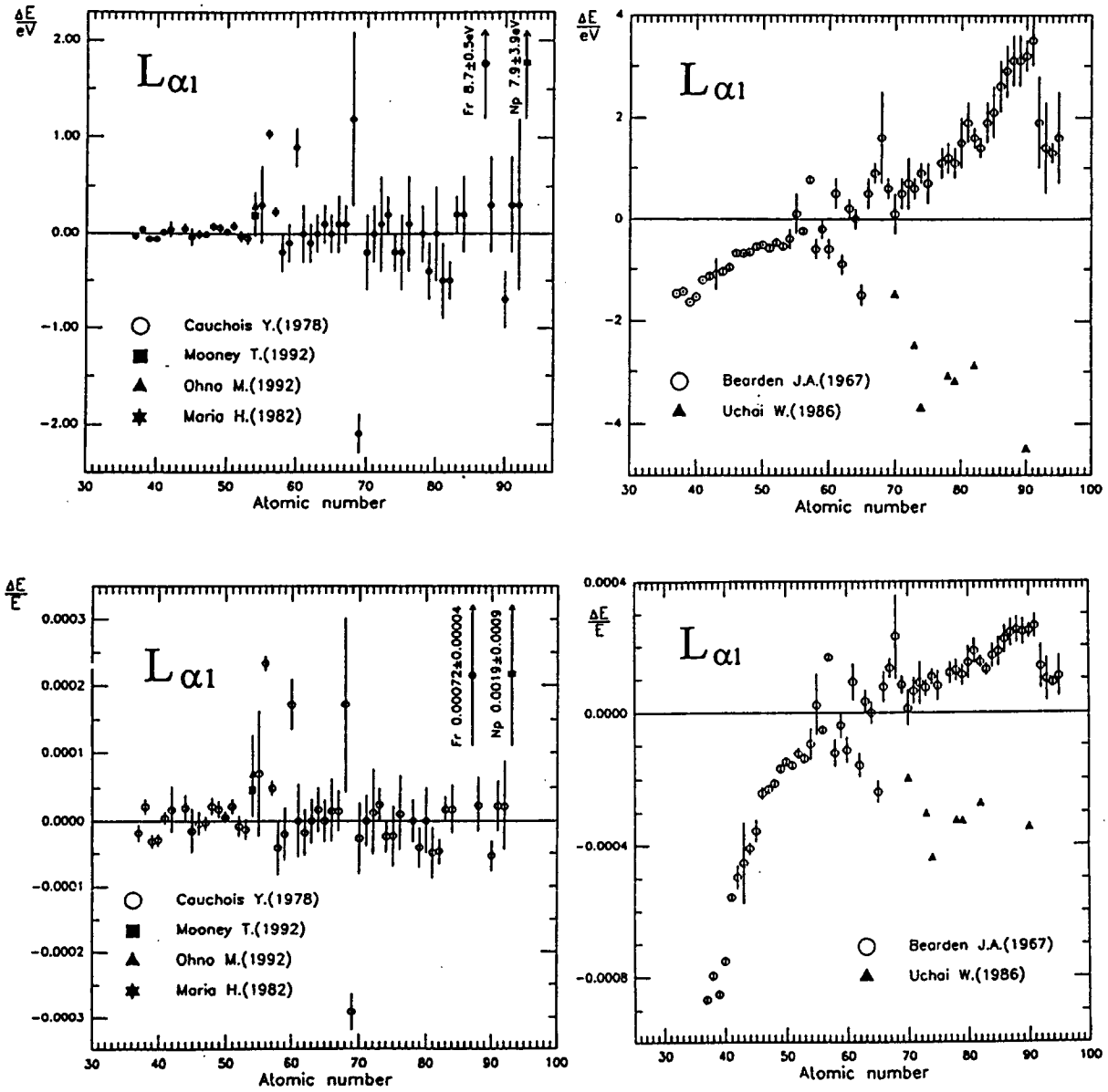

Figure 1: Differences ΔE of experimentally or theoretically determined L_{α_1} transition energies E from experimental values of Bearden [2] (left side of the Fig.) and theoretical ones from Huang et al. [7] (right side of the Fig.).

4. Electron Shake-Off Probabilities for Elements with $Z \leq 60$

A.M.El-Shimy [1], G.Zschornack

Through a sudden change of the atomic potential, for example due to an ionization process, electrons can be ionized from a bound state in the continuum. Usually this monopol transition is marked as electron shake-off. The electron shake-off probabilities are described according to Åberg [1, 2] by overlap integrals between the wave functions of the initial state Φ_i and the final state Φ_f of the considered process.

Shake-off probabilities are required for the characterization of a series of phenomena in atomic physics, for instance the modelling of vacancy cascades in atoms after inner-shell ionization [3]. Known are calculations of Carlson and Nestor [4] and Mukoyama and Taniguchi [5, 6] for the determination of the shake-off probabilities of noble gases (Ne, Ar, Kr, Xe) using Hartree-Fock-Slater wave functions. We accomplished analogous calculations on the basis of Dirac-Fock-Slater wave functions in the region $10 \leq Z \leq 60$. Results are available as tables and as computer files.

The calculations proceeded on the assumption, that Φ_i and Φ_f are presented as Slater determinants

$$\Phi = \frac{1}{\sqrt{N!}} \begin{vmatrix} u_1(r_1) & u_1(r_2) & u_1(r_3) & \dots & u_1(r_N) \\ u_2(r_2) & u_2(r_2) & u_2(r_3) & \dots & u_2(r_N) \\ u_3(r_1) & u_3(r_2) & u_3(r_3) & \dots & u_3(r_N) \\ \vdots & \vdots & \vdots & & \vdots \\ u_N(r_1) & u_N(r_2) & u_N(r_3) & \dots & u_N(r_N) \end{vmatrix} \tag{1}$$

with N as electron number. With it the probability for an electron transition from the orbital nlj in the orbital $n'l'j'$ yields

$$P_{nlj \to n'l'j'} = \left| \int u^*_{n'l'j'}(A_0)\, u_{nlj}(A)\, d\tau \right|^2 \tag{2}$$

with $u_{nlj}(A)$ and $u^*_{n'l'j'}(A_0)$ as orbital wave functions for the orbital nlj in the neutral atom A and for the orbital $n'l'j'$ in the ion A_0. Thereby the ion originates from the atom A during a change in the potential in the course of ionization processes. The probability, that at least one from N electrons, which are located in the sub-shell nlj, is ionized, totals

$$P = 1 - \left(\left| \int u^*_{nlj}(A_0)\, u_{nlj}(A)\, d\tau \right|^2 \right)^N - P_f \tag{3}$$

If the electron is emitted from the orbital nlj, it is either ionized in the continuum (electron shake-off) or populates a bound state (electron shake-up). In the calculation of the electron shake-off process the possibility must be excluded that transitions occur to occupied sub-shells, since such transitions are not allowed according to the Pauli exclusion principle. The size P_f is a correction for physically not allowed transitions to occupied shells and has the form

[1] permanent address: El-Minia University, Department of Physics, El-Minia, Egypt

$$P_f = \sum_{n'lj} N \frac{N'}{2j+1} \left| \int u^*_{n'lj}(A_0)\, u_{n'lj}(A)\, d\tau \right|^2 \tag{4}$$

with $n' \neq n$ and N' as number of the electrons in the orbital $n'lj$.

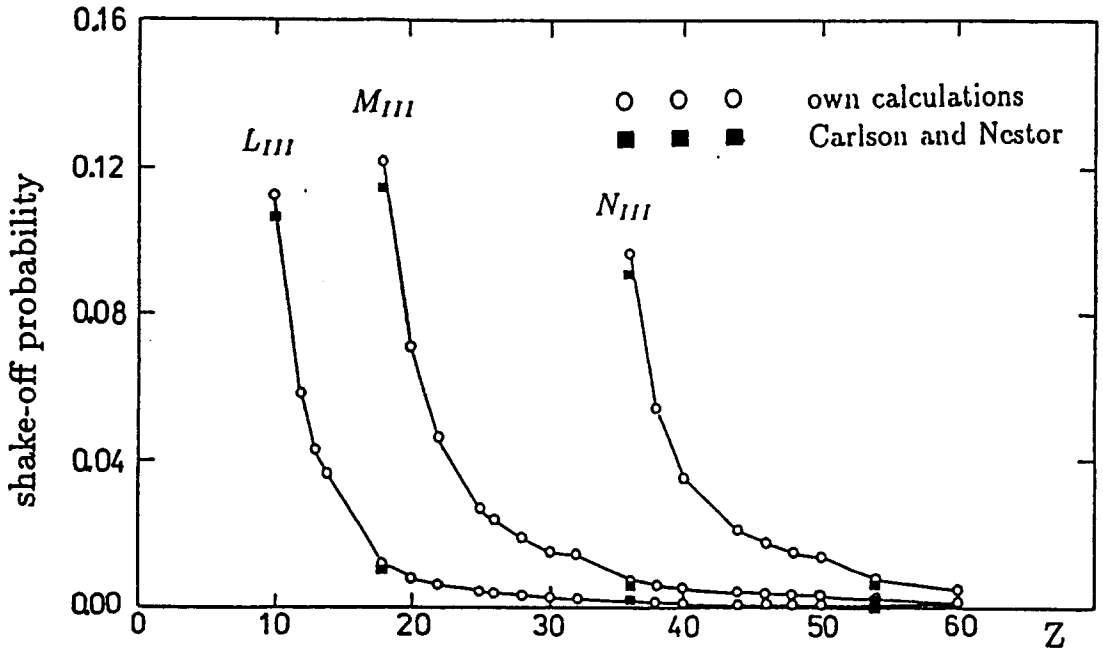

Figure 1: Shake-off probabilities as a function of the atomic number Z for the emission of an electron from the L_{III}, M_{III} and N_{III} sub-shells after the production of an inner-shell vacancy.

As an example of the accomplished calculations we show in Fig.1 the dependence of the shake-off probability from the atomic number Z for the emission of an electron from selected sub-shells after the production of a primary K-vacancy in this shell. A good agreement is observed with the values of Carlson and Nestor [4].

This work has been supported by BMFT under contract No. 06 DD 111.

References

[1] T.Åberg; Physical Review, 156 (1967) 35

[2] T.Åberg; Ann. Acad. Sci. Finn. Ser. AVI Physica, 308 (1969) 7

[3] A.M.M.Mohammedein, I.Reiche, G.Zschornack; Radiation Effects and Defects in Solids, 126 (1993) 309

[4] A.Carlson, C.W.Nestor; Physical Review, A8 (1973) 2887

[5] T.Mukoyama, K.Taniguchi; Physical Review, A36 (1987) 1

[6] T.Mukoyama, K.Taniguchi; Bull. Inst. Chem. Res., Kyoto University, 70 (1992) 1

5. Nuclear Model Calculations on Measured Isomeric Cross-Section Ratios for ^{75m,g}Ge

I. Birn

In the previous issues of this report experimental studies on fast neutron induced threshold reaction cross sections and isomeric cross section ratios were described. The experiments were done in collaboration with the Forschungszentrum Jülich, Institut für Nuklearchemie. In continuation of those studies nuclear model calculations were performed.

a) Within the framework of the statistical model, the code STAPRE [1] was used. For the emission of the first particle a width-fluctuation corrected Hauser-Feshbach formula was applied and pre-equilibrium emission was taken into account (exciton model). For higher chance emission, the evaporation formula was used. The model calculations were done in collaboration with the University of Vienna, Institut für Radiumforschung und Kernphysik.

b) The statistical multistep direct/statistical multistep compound model was used (code EXIFON [2]).

These calculations were done for the isomeric pair ^{75m,g}Ge in (n,p), (n,2n) and (n,α) reactions. The excitation functions are described well by the model calculations; the agreement of the calculated isomeric cross section ratios with the experimental values is excellent. As an example the isomeric cross section ratio of ^{75m,g}Ge in the (n,p) reaction is given (see Fig. 1. η denotes the ratio of the effective moment of inertia to the rigid body moment of inertia). Calculations for the ^{72,74}Ge(n,α)^{69m,71m}Zn reactions are in progress. Detailed results will be published elsewhere.

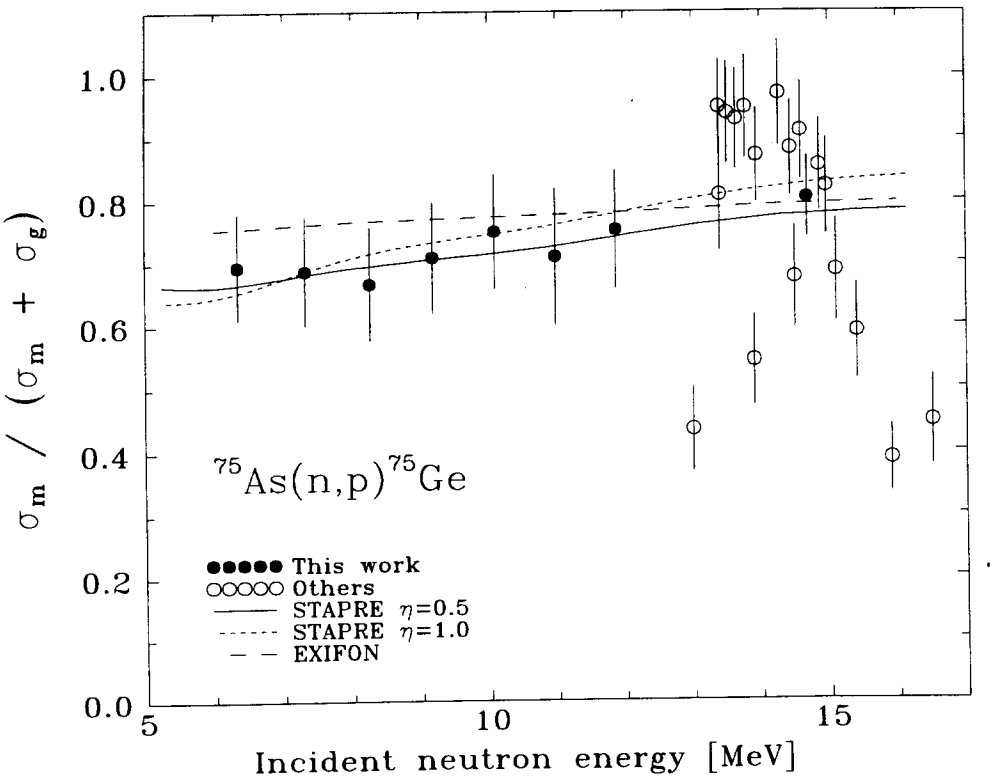

Fig 1 Comparison of experimental and theoretical isomeric cross section ratio for the isomeric pair ^{75m,g}Ge formed via (n,p) reaction on ^{75}As

[1] M. Uhl und B. Strohmaier, "STAPRE: A Computer Code for Particle Induced Activation Cross Sections and Related Quantities", IRK 76/01 und Addenda, Institut für Radiumforschung und Kernphysik, Wien (1976, Upd. 1981).

[2] H. Kalka, "EXIFON - A Statistical Multistep Reaction Code", NEA Data Bank, Saclay, France (1991).

ABTEILUNG NUKLEARCHEMIE
UNIVERSITÄT ZU KÖLN
AND
ZENTRUM FÜR STRAHLENSCHUTZ UND RADIOÖKOLOGIE
UNIVERSITÄT HANNOVER

1. Production of Radionuclides from Target Elements (Z < 30) by Proton-Induced Reactions between 200 and 400 MeV

M. Gloris[1], I. Leya[1], R. Michel[2], T. Schiekel[2], U. Herpers[2], B. Dittrich-Hannen[3], H.-A. Synal[3], M. Suter[3], P.W. Kubik[4]

Cross sections for the production of residual nuclides by p-induced reactions are the basic nuclear quantities needed for an accurate modelling of the interaction of cosmic ray protons with matter. Moreover, medium-energy nuclear data are of interest for a large range of other applications [1], in particular, for feasibility studies of accelerator-based waste transmutation and energy amplification systems.

In the course of a large project to measure cosmochemically relevant thin-target cross sections for proton-induced reactions [2-13, and references therein], we here report on experiments, which fill an energy gap in most excitation functions between 200 MeV and 400 MeV. In two experiments at Laboratoire National Saturne (LNS)/Saclay nineteen target elements (C, N, O, Mg, Al, Si, Ca, Ti, Mn, Fe, Co, Ni, Cu, Sr, Y, Zr, Nb, Ba and Au) were irradiated with 300 and 400 MeV protons. The stacked-foil technique was used, with two stacks arranged in a line in each experiment. The thicknesses of the stacks

1 Zentrum für Strahlenschutz und Radioökologie, Universität Hannover, F.R.G.
2 Abteilung Nuklearchemie, Universität zu Köln, F.R.G.
3 Inst. für Teilchenphysik, ETH-Hönggerberg, Zürich, Switzerland
4 Paul Scherrer Insitut, c/o Institut für Teilchenphysik, ETH-Hönggerberg, Zürich, Switzerland

were chosen so that energy ranges from 400 MeV to 300 MeV and from 300 MeV to 200 MeV, respectively, were covered. For each target element multiple foils were irradiated. In order to avoid recoil losses and contamination, only foils in the middle were analyzed. At least four energy points were investigated for each target element between 400 MeV and 200 MeV.

Residual nuclides were measured by γ-ray spectrometry and by accelerator mass spectrometry (AMS). The γ-ray spectrometric methods and the experimental techniques for the separation of the long-lived isotopes for AMS were identical to those used earlier [2, 3, 6, 12]. $^{10}Be/^{9}Be$, $^{26}Al/^{27}Al$ and $^{36}Cl/Cl$ ratios were measured at the PSI-ETH AMS-facility in Zürich [14]. The standards used for the AMS measurements were "S555" with a $^{10}Be/^{9}Be$ ratio of $95.5 * 10^{-12}$, "A1092" with a $^{26}Al/^{27}Al$ ratio of $133.07 * 10^{-12}$ and "K380/4" with a $^{36}Cl/Cl$ ratio of $15.3 * 10^{-12}$.

The proton energy in each individual target foil was calculated according to the work of Andersen and Ziegler [15]. The beam current was monitored by the reactions $^{27}Al(p,3p3n)^{22}Na$ using the recommended cross sections from the evaluation by Tobailem and de Lassus St. Genies [16]. In order to correct for contributions of secondary protons and neutrons, the spectra of secondary protons and neutrons were calculated for each stack by the HERMES [17] code system. The contributions of the secondary particles were calculated by folding these spectra with thin-target cross sections of p- and n-induced reactions as described by Lüpke [18].

In this work, we report on target elements $Z \leq 30$. The new cross sections for the production of short- and medium-lived γ-emitting radionuclides are presented in Table 1, those for ^{10}Be, ^{26}Al and ^{36}Cl in Table 2.

Acknowledgement The authors thank the authorities of Laboratoire National Saturne/Saclay for the beam-time and the accelerator staffs for their cooperation. This work was suported by the Deutsche Forschungsgemeinschaft.

References

[1] N.P. Kocherov (ed.) Intermediate energy nuclear data for applications, INDC(NDS)-245, IAEA, Vienna, (1991)

[2] R. Michel and R. Stück, Proc. 14th Lun. Plan. Sci. Conf., J. Geophys. Res. 89 (1984) B673

[3] R. Michel, F. Peiffer and R. Stück, Nucl. Phys. A 441 (1985) 617

[4] R. Michel, B. Dittrich, U. Herpers, T.Schiffmann, P. Cloth, P. Dragovitsch, D. Filges, Analyst 114 (1989) 287

[5] B. Dittrich, U. Herpers, M. Lüpke, R. Michel, in: Progress Report on Nuclear Data Research in the Federal Republic of Germany for the Period April, 1st, 1988 to March, 31st, 1989, NEANDC(E)-302 U Vol. V INDC(Ger)-34/LN + Special, 1989, 31

[6] B. Dittrich, U. Herpers, H.J. Hofmann, W. Wölfli, R. Bodemann, M. Lüpke, R. Michel, P. Dragovitsch, D. Filges, Nucl. Instr. Meth. Phys. Res. B52 (1990) 588

[7] B. Dittrich, U. Herpers, R. Bodemann, M. Lüpke, R. Michel, P. Signer, R. Wieler, H.J. Hofmann, W. Wölfli, in: Progress Report on Nuclear Data Research in the Federal Republic of Germany for the Period April, 1st, 1989 to March, 31st, 1990, NEANDC(E)-312-U Vol. V INDC(Ger)-35/LN + Special, 1990, 45

[8] B. Dittrich, U. Herpers, R. Bodemann, R. Michel, H. Condé, B. Holmqvist, P. Malmborg, in: Progress Report on Nuclear Data Research in the Federal Republic of Germany for the Period April, 1st, 1989 to March, 31st, 1990, NEANDC(E)-312-U Vol. V INDC(Ger)-35/LN + Special, 1990, 57

[9] M. Lüpke, R. Michel, B. Dittrich, U. Herpers,P. Dragovitsch, D. Filges, H.J. Hofmann, W. Wölfli, in: S.M. Qaim (ed.): Nuclear Data for Science and Technology, Springer Verlag, Berlin (1992) 702

[10] R. Bodemann, R. Michel, B. Dittrich, U. Herpers, R. Rösel, H.J. Hofmann, W. Wölfli, B. Holmqvist, H. Condé, P. Malmborg, in: S.M. Qaim (ed.): Nuclear Data for Science and Technology, Springer Verlag, Berlin (1992) 705

[11] M. Lüpke, H.-J. Lange, M. Schnatz-Büttgen, R. Michel, R. Rösel, U. Herpers, P. Cloth, D. Filges, in: Progress Report on Nuclear Data Research in the Federal Republic of Germany for the Period April, 1st, 1991 to

March, 31st, 1992, NEA/NSC/DOC(92)5, INDC(Ger)-036/L, KFK 5079, 1992, 51

[12] R. Bodemann, H.-J. Lange, R. Michel, T. Schiekel, R. Rösel, U. Herpers, H.J. Hofmann, B. Dittrich, M. Suter, W. Wölfli, B. Holmqvist, H. Condé, P. Malmborg, Nucl. Instr. Meth. Phys. Res. B82 (1993) 9

[13] R. Bodemann, H.-J. Lange, I. Leya, R. Michel, T. Schiekel, R. Rösel, U. Herpers, H. J. Hofmann, B. Dittrich, M. Suter, W. Wölfli, B. Holmqvist, H. Condé, P. Malmborg, in: Progress Report on Nuclear Data Research in the Federal Republic of Germany for the Period April, 1st, 1992 to March, 31st, 1993, NEA/NSC/DOC(93)17, INDC(Ger)-037/LN, 49, Jül-2803

[14] M. Suter, R. Balzer, G. Bonani, H.J. Hofmann, M. Morenzoni, M. Nessi, W. Wölfli, M. Andree, J. Beer, and H. Oeschger, Nucl. Instr. Meth. Phys. Res. B5 (1984) 117

[15] H.H. Andersen and J.F. Ziegler, Hydrogen Stopping Powers in All Elements, Pergamon Press (1977)

[16] J. Tobailem and C.H. de Lassus St. Genies, CEA-N-1466(5) (1981)

[17] P. Cloth, D. Filges, R.D. Neef, G. Sterzenbach, Ch. Reul, T.W. Armstrong, B.L. Colborn, B. Anders and H. Brueckmann, Juel-2203 (1988)

[18] M. Lüpke, Thesis, Universität Hannover (1993)

Table 1: Cross sections [mb] for proton-induced reactions on C, N, O, Mg, Al, Si, Ti, Mn, Fe, Co, Ni, Cu measured by γ-ray spectrometry. All cross sections are cumulative, except for those indicated by "i", which are independent cross sections.

Energy	256 MeV	298 MeV	363 MeV	398 MeV
C(p,3pXn)^{7}Be	10.4 ± 0.6	11.1 ± 0.6	11.0 ± 0.6	11.8 ± 0.7

Energy	248 MeV	290 MeV	356 MeV	392 MeV
N(p,4pXn)^{7}Be	9.13 ± 0.60	10.1 ± 0.6	10.4 ± 0.8	11.3 ± 0.7

Energy	254 MeV	296 MeV	361 MeV	396 MeV
Mg(p,9pXn)^{7}Be	3.14 ± 0.18	3.68 ± 0.20	4.22 ± 0.22	4.81 ± 0.27
Mg(p,2pXn)^{22}Na	33.9 ± 1.9	34.5 ± 1.8	33.0 ± 1.7	34.0 ± 1.8
Mg(p,2pXn)^{24}Na	5.36 ± 0.31	5.36 ± 0.30	5.72 ± 0.32	6.02 ± 0.35

Energy	256 MeV	297 MeV	362 MeV	398 MeV
Al(p,10p11n)^{7}Be	1.82 ± 0.12	2.29 ± 0.13	2.86 ± 0.22	3.34 ± 0.27
Al(p,3p3n)^{22}Na	14.3 ± 0.8	15.4 ± 0.8	15.7 ± 1.3	16.1 ± 1.0
Al(p,3pn)^{24}Na	9.74 ± 0.55	10.5 ± 0.6	11.3 ± 0.9	11.7 ± 1.1

Energy	252 MeV	294 MeV	359 MeV	395 MeV
Si(p,11pXn)^{7}Be	2.06 ± 0.11	2.53 ± 0.13	3.20 ± 0.17	3.60 ± 0.27
Si(p,4pXn)^{22}Na	16.0 ± 0.9	17.0 ± 0.9	17.5 ± 0.9	18.3 ± 0.3
Si(p,4pXn)^{24}Na	3.75 ± 0.21	4.22 ± 0.22	4.31 ± 0.23	4.79 ± 0.22
Si(p,3pXn)^{28}Mg	0.0435± 0.0067	0.0503 ± 0.0063	0.0603 ± 0.0078	0.0629 ± 0.0048

Energy	241 MeV	284 MeV	350 MeV	386 MeV
Ti(p,19pXn)^{7}Be	0.601 ± 0.062	0.787 ± 0.056	0.972 ± 0.062	1.13 ± 0.078
Ti(p,12pXn)^{22}Na	0.125 ± 0.015	0.201 ± 0.025	0.300 ± 0.024	0.383 ± 0.031
Ti(p,4pXn)^{43} K	2.97 ± 0.28	3.12 ± 0.21	3.42 ± 0.26	3.62 ± 0.27
Ti(p,3pXn)^{47}Ca	0.147 ± 0.014	0.174 ± 0.011	0.205 ± 0.013	0.214 ± 0.014
Ti(p,2pXn)^{44m}Sc	9.57 ± 0.65	8.93 ± 0.46	8.72 ± 0.47	8.40 ± 0.46
Ti(p,2pXn)^{46}Sc	30.2 ± 2.1	30.3 ± 1.6	31.0 ± 1.6	31.0 ± 1.7
Ti(p,2pXn)^{47}Sc	21.6 ± 1.5	22.0 ± 1.2	23.7 ± 1.3	24.1 ± 1.4
Ti(p,2pXn)^{48}Sc	2.12 ± 0.16	2.13 ± 0.13	2.35 ± 0.15	2.28 ± 0.15
Ti(p,Xn)^{48}V	1.92 ± 0.16	1.62 ± 0.12	1.35 ± 0.11	1.35 ± 0.11

Table 1: (continued)

Energy	239 MeV	282 MeV	348 MeV	384 MeV
Mn(p,22p27n)^{7}Be	-	0.876 ± 0.204	0.981 ± 0.245	1.23 ± 0.30
Mn(p,15p19n)^{22}Na	0.0373± 0.0068	0.0665 ± 0.0133	0.103 ± 0.012	0.130 ± 0.014
Mn(p,7p6n)^{43}K	0.888 ± 0.105	1.05 ± 0.10	1.30 ± 0.11	1.60 ± 0.14
Mn(p,6p3n)^{47}Ca	0.0256± 0.0060	0.0356 ± 0.0053	0.0613 ± 0.0062	0.0720 ± 0.0090
Mn(p,5p7n)^{44m}Sc	5.27 ± 0.41	5.98 ± 0.46	6.27 ± 0.48	7.46 ± 0.60
Mn(p,5p5n)^{46}Sc	9.67 ± 0.77	10.9 ± 0.8	11.7 ± 0.9	13.0 ± 1.0
Mn(p,5p4n)^{47}Sc	5.30 ± 0.41	6.06 ± 0.47	5.97 ± 0.45	6.61 ± 0.52
Mn(p,3p5n)^{48}V^{i}	19.0 ± 1.7	19.7 ± 1.8	18.9 ± 1.7	19.7 ± 1.9
Mn(p,2p6n)^{48}Cr	0.488 ± 0.109	0.534 ± 0.105	0.487 ± 0.104	0.567 ± 0.101
Mn(p,2p3n)^{51}Cr	53.8 ± 4.3	59.1 ± 7.5	47.0 ± 3.7	47.4 ± 4.0
Mn(p,p3n)^{52}Mn	10.3 ± 0.9	9.58 ± 0.8	7.83 ± 0.66	7.56 ± 0.74
Mn(p,pn)^{54}Mn	57.6 ± 4.7	57.0 ± 4.8	51.6 ± 4.2	54.3 ± 4.8

Energy	236 MeV	299 MeV	346 MeV	399 MeV
Fe(p,23pXn)^{7}Be	0.503 ± 0.165	0.821 ± 0.128	0.874 ± 0.116	1.17 ± 0.12
Fe(p,16pXn)^{22}Na	-	0.0558 ± 0.0071	0.0848 ± 0.0088	0.131 ± 0.012
Fe(p,8pXn)^{43}K	-	0.504 ± 0.050	-	0.757 ± 0.068
Fe(p,6pXn)^{44m}Sc	4.58 ± 0.36	5.61 ± 0.40	6.68 ± 0.50	7.1 ± 0.5
Fe(p,6pXn)^{46}Sc	5.51 ± 0.43	6.84 ± 0.49	7.32 ± 0.54	8.77 ± 0.63
Fe(p,6pXn)^{47}Sc	1.78 ± 0.14	2.19 ± 0.16	2.43 ± 0.18	2.71 ± 0.20
Fe(p,4pXn)^{48}V^{i}	20.2 ± 1.9	21.0 ± 1.7	22.7 ± 2.0	24.4 ± 1.9
Fe(p,3pXn)^{48}Cr	1.01 ± 0.21	1.07 ± 0.08	0.809 ± 0.218	1.14 ± 0.09
Fe(p,3pXn)^{51}Cr	53.8 ± 4.23	54.2 ± 3.9	52.1 ± 3.9	51.5 ± 3.7
Fe(p,2pXn)^{52}Mn	15.8 ± 1.3	15.1 ± 1.1	14.2 ± 1.1	13.9 ± 1.0
Fe(p,2pXn)^{54}Mn	42.4 ± 3.4	42.5 ± 3.1	41.1 ± 3.1	42.4 ± 3.0
Fe(p,Xn)^{55}Co	-	1.01 ± 0.19	-	0.947 ± 0.244
Fe(p,Xn)^{56}Co	1.50 ± 0.14	1.33 ± 0.094	1.06 ± 0.10	1.09 ± 0.08
Fe(p,Xn)^{57}Co	0.192 ± 0.016	0.119 ± 0.010	0.212 ± 0.017	0.147 ± 0.012
Fe(p,Xn)^{58}Co	0.0259± 0.0083	0.0291 ± 0.0065	0.0365 ± 0.0079	0.0291 ± 0.0067

Energy	233 MeV	277 MeV	343 MeV	380 MeV
Co(p,24p29n)^{7}Be	-	0.587 ± 0.214	0.706 ± 0.161	0.719 ± 0.188
Co(p,17p21n)^{22}Na	0.0168± 0.0051	0.0269 ± 0.0062	0.0475 ± 0.0072	0.0761 ± 0.0078
Co(p,7p9n)^{44m}Sc	2.09 ± 0.18	2.94 ± 0.23	3.89 ± 0.30	4.93 ± 0.38
Co(p,7p7n)^{46}Sc	3.47 ± 0.30	4.63 ± 0.36	5.86 ± 0.46	6.91 ± 0.53
Co(p,7p6n)^{47}Sc	1.57 ± 0.14	1.93 ± 0.15	2.42 ± 0.19	2.82 ± 0.22
Co(p,5p7n)^{48}V	10.7 ± 0.9	12.9 ± 1.0	14.1 ± 1.1	15.8 ± 1.2
Co(p,4p5n)^{51}Cr	34.8 ± 3.0	37.9 ± 3.0	36.8 ± 2.9	39.8 ± 3.1
Co(p,3p5n)^{52}Mn	12.8 ± 1.1	13.1 ± 1.1	12.5 ± 1.0	13.1 ± 1.0
Co(p,3p3n)^{54}Mn	35.3 ± 3.1	36.7 ± 2.9	36.1 ± 2.8	37.5 ± 2.9
Co(p,p3n)^{56}Co	13.9 ± 1.2	13.2 ± 1.1	11.2 ± 0.9	11.0 ± 0.9
Co(p,p2n)^{57}Co^{i}	43.4 ± 4.0	41.5 ± 3.4	38.2 ± 3.2	38.2 ± 3.2
Co(p,pn)^{58}Co	58.6 ± 5.3	57.1 ± 4.8	54.8 ± 4.7	56.5 ± 4.8
Co(p,3n)^{57}Ni	0.714 ± 0.080	0.663 ± 0.063	0.447 ± 0.056	0.499 ± 0.051

Table 1: continued

Energy	230 MeV	275 MeV	341 MeV	378 MeV
Ni(p,25pXn)^{7}Be	-	0.528 ± 0.193	0.930 ± 0.263	1.31 ± 0.28
Ni(p,18pXn)^{22}Na	-	-	0.087 ± 0.014	0.102 ± 0.016
Ni(p,8pXn)^{44m}Sc	2.49 ± 0.22	3.47 ± 0.27	4.44 ± 0.35	5.42 ± 0.41
Ni(p,8pXn)^{46}Sc	1.72 ± 0.15	2.42 ± 0.18	3.07 ± 0.24	3.61 ± 0.27
Ni(p,6pXn)^{48}V^{i}	14.2 ± 1.5	16.7 ± 1.5	18.2 ± 1.8	20.2 ± 1.9
Ni(p,5pXn)^{48}Cr	0.826 ± 0.231	1.40 ± 0.16	1.40 ± 0.27	1.65 ± 0.20
Ni(p,5pXn)^{51}Cr	38.0 ± 3.2	42.7 ± 3.2	41.9 ± 3.3	44.3 ± 3.4
Ni(p,4pXn)^{52}Mn	17.8 ± 1.5	19.0 ± 1.4	17.9 ± 1.4	18.7 ± 1.4
Ni(p,4pXn)^{54}Mn	17.2 ± 1.5	18.6 ± 1.4	17.5 ± 1.4	17.6 ± 1.4
Ni(p,3pXn)^{59}Fe	0.237 ± 0.060	0.232 ± 0.047	0.226 ± 0.045	0.250 ± 0.041
Ni(p,2pXn)^{56}Co^{i}	42.4 ± 4.2	42.7 ± 3.7	37.7 ± 3.5	39.0 ± 3.5
Ni(p,2pXn)^{57}Co^{i}	42.6 ± 9.1	46.1 ± 8.6	44.2 ± 8.4	42.7 ± 7.7
Ni(p,2pXn)^{58}Co	11.7 ± 1.3	13.4 ± 1.4	12.3 ± 1.4	12.2 ± 1.4
Ni(p,2pXn)^{60}Co	1.28 ± 0.13	1.50 ± 0.14	1.39 ± 0.14	1.47 ± 0.14
Ni(p,pXn)^{56}Ni	3.33 ± 0.32	3.40 ± 0.26	2.91 ± 0.24	2.94 ± 0.23
Ni(p,pXn)^{57}Ni	31.4 ± 2.7	33.0 ± 2.5	28.0 ± 2.3	26.5 ± 2.1

Energy	226 MeV	271 MeV	338 MeV	375 MeV
Cu(p,26pXn)^{7}Be	0.288 ± 0.114	0.544 ± 0.136	0.733 ± 0.153	-
Cu(p,19pXn)^{22}Na	-	-	0.0323 ± 0.0082	0.0445 ± 0.0062
Cu(p,9pXn)^{44m}Sc	0.448 ± 0.042	0.809 ± 0.068	1.51 ± 0.12	1.87 ± 0.15
Cu(p,9pXn)^{46}Sc	0.851 ± 0.066	1.43 ± 0.11	2.34 ± 0.18	2.87 ± 0.22
Cu(p,9pXn)^{47}Sc	0.538 ± 0.043	0.789 ± 0.063	1.17 ± 0.092	1.37 ± 0.10
Cu(p,7pXn)^{48}V	3.13 ± 0.24	4.63 ± 0.36	6.54 ± 0.50	7.65 ± 0.58
Cu(p,6pXn)^{51}Cr	13.4 ± 1.1	17.3 ± 1.4	20.8 ± 1.6	22.8 ± 1.7
Cu(p,5pXn)^{52}Mn	5.87 ± 0.45	7.13 ± 0.56	8.18 ± 0.63	8.67 ± 0.66
Cu(p,5pXn)^{54}Mn	17.7 ± 1.4	19.7 ± 1.6	21.5 ± 1.7	22.3 ± 1.7
Cu(p,4pXn)^{59}Fe	1.12 ± 0.09	1.25 ± 0.11	1.39 ± 0.12	1.49 ± 0.12
Cu(p,3pXn)^{56}Co	11.1 ± 0.87	12.0 ± 1.0	11.4 ± 0.9	11.4 ± 0.9
Cu(p,3pXn)^{57}Co^{i}	33.9 ± 2.9	34.9 ± 3.1	32.6 ± 2.8	32.6 ± 2.8
Cu(p,3pXn)^{58}Co	39.4 ± 3.1	40.3 ± 3.2	38.5 ± 3.0	38.0 ± 3.0
Cu(p,3pXn)^{60}Co	8.78 ± 0.72	9.23 ± 0.76	9.52 ± 0.78	9.66 ± 0.79
Cu(p,2pXn)^{56}Ni	-	0.115 ± 0.040	0.109 ± 0.040	0.0777 ± 0.0319
Cu(p,2pXn)^{57}Ni	1.64 ± 0.14	1.64 ± 0.14	1.53 ± 0.13	1.50 ± 0.12
Cu(p,Xn)^{65}Zn	0.790 ± 0.077	0.647 ± 0.069	0.581 ± 0.062	0.562 ± 0.063
Cu(p,n)^{65}Zn	2.56 ± 0.25	2.10 ± 0.22	1.89 ± 0.20	1.82 ± 0.21

Table 2: Cross sections [mb] for proton-induced reactions on C, N, O, Mg, Al, Si, Ca, Ti, Fe, Co and Ni measured by accelerator mass spectrometry. All cross sections are cumulative. The uncertainties in the proton-energies are between 0.6 MeV and 1.8 MeV.

Energy MeV	Cross Section mb	Energy MeV	Cross Section mb
C(p,3pXn)^{10}Be		Al(p,pn)^{26}Al	
256.	1.94 ± 0.18	256.	26.1 ± 2.3
298.	2.31 ± 0.19	298.	27.1 ± 2.4
363.	2.7 ± 0.2	362.	27.4 ± 2.5
398.	3.05 ± 0.25	398.	26.8 ± 2.3
N(p,4pXn)^{10}Be		Si(p,2pXn)^{26}Al	
249.	0.808 ± 0.067	249.	23.5 ± 1.1
291.	1.17 ± 0.10	291.	22.8 ± 0.8
356.	1.07 ± 0.09	294.	23.7 ± 2.4
392.	1.16 ± 0.10	356.	20.2 ± 0.9
		358.	22.7 ± 1.9
O(p,5pXn)^{10}Be		392.	21.8 ± 0.8
245.	0.915 ± 0.109	394.	22.6 ± 1.8
288.	1.21 ± 0.15		
353.	1.44 ± 0.19	Ca(p,8pXn)^{26}Al	
389.	1.62 ± 0.19	243.	3.49 ± 0.50
		286.	5.23 ± 0.62
Mg(p,9pXn)^{10}Be		351.	4.92 ± 1.29
254.	0.438 ± 0.027	387.	7.07 ± 0.58
295.	0.545 ± 0.023		
360.	0.701 ± 0.037	Fe(p,14pXn)^{26}Al	
396.	0.832 ± 0.034	237.	0.038 ± 0.016
		280.	0.057 ± 0.026
Al(p,10p8n)^{10}Be		382.	0.208 ± 0.028
256.	0.359 ± 0.034		
298.	0.550 ± 0.051	Ca(p,4pXn)^{36}Cl	
362.	0.713 ± 0.065	243.	14.0 ± 1.4
398.	0.852 ± 0.080	351.	13.8 ± 1.9
		387.	13.9 ± 1.3
Si(p,11pXn)^{10}Be			
252.	0.194 ± 0.008	Ti(p,6pXn)^{36}Cl	
294.	0.276 ± 0.011	242.	6.73 ± 0.62
358.	0.386 ± 0.020	285.	8.14 ± 0.75
394.	0.510 ± 0.025	350.	10.1 ± 1.0
		387.	11.4 ± 1.1
Ti(p,19pXn)^{10}Be			
386.	0.287 ± 0.029	Fe(p,10pXn)^{36}Cl	
		236.	0.874 ± 0.080
Fe(p,23pXn)^{10}Be		237.	0.733 ± 0.067
236.	0.088 ± 0.009	280.	1.20 ± 0.11
237.	0.100 ± 0.016	346.	2.28 ± 0.21
280.	0.101 ± 0.010		
345.	0.195 ± 0.019	Co(p,11pXn)^{36}Cl	
346.	0.178 ± 0.019	233.	0.26 ± 0.023
382.	0.209 ± 0.022	278.	0.623 ± 0.051
		344.	1.31 ± 0.11
Ni(p,25pXn)^{10}Be		380.	1.74 ± 0.14
231.	0.035 ± 0.009		
275.	0.069 ± 0.007	Ni(p,12pXn)^{36}Cl	
341.	0.111 ± 0.011	275.	0.651 ± 0.046
378.	0.142 ± 0.014	341.	1.18 ± 0.08
		378.	1.85 ± 0.15
Mg(p,Xn)^{26}Al			
254.	0.119 ± 0.014		
295.	0.139 ± 0.016		
360.	0.102 ± 0.012		
396.	0.064 ± 0.008		

INSTITUT FÜR KERNCHEMIE
UNIVERSITÄT MAINZ

Mass, Charge and Energy Distributions in the Very Asymmetric Fission of ^{249}Cf Induced by Thermal Neutrons

R. Hentzschel, H. R. Faust[1], H. O. Denschlag, B. D. Wilkins[2], J. Gindler[2]

Fission yields of fragments with mass numbers A=69-87 and fragment kinetic energies for A=74-87 in the very asymmetric neutron induced fission of ^{249}Cf have been measured using the mass separator Lohengrin at the Institut Laue-Langevin in Grenoble. The chain yields observed in this very light mass region are considerably higher than predicted. An evaluation of the isotopic yields shows a strong increase of the proton odd-even effect from 7 % to 17 % with increasingly asymmetric fission. The neutron odd-even effect is increasing from 4 % to 10 %. These observations and a narrowing of the average nuclear charge distribution can be explained by a decreasing excitation energy with increasing asymmetry of the fission process.

This work has appeared in Nuclear Physics A571, 427-446 (1994)

---

[1]Institut Laue-Langevin, 156X, F-38042 Grenoble, France
[2]Argonne National Laboratory, Argonne, IL 60439, USA

INSTITUT FÜR KERNCHEMIE
PHILIPPS-UNIVERSITÄT MARBURG

^{252}Cf : Neutron Multiplicities in Correlation with Fission Fragment Mass and Energy §

J. van Aarle, W. Westmeier, R.A. Esterlund and P. Patzelt

Following the development in 1983 of the *multi-modal random neck-rupture model* of Brosa et al., the theoretical description of the fission process has made significant gains. For the spontaneous fission of ^{252}Cf, Brosa et al. predict not less than six different fission channels, not all of which have to date been verified experimentally. Making use of the extremely high counting efficiency of our scintillator tank for neutrons, we attempt here to verify if these predicted fission channels do indeed exist.

We assayed coincident fission fragment energies and neutron multiplicities for ca. 1.7 x 10^7 spontaneous fission events of ^{252}Cf. The neutrons were detected with an efficiency of ca. 85%. In Figure 1, we show our three-dimensional matrix of the number of events as a function of fragment mass (A) and total kinetic energy (TKE) for the spontaneous fission of ^{252}Cf. The figure covers the assayed range in masses and TKE and exhibits the well-known double-humped yield distribution. It should be noted that we did not discard any information which might originate from rare fission channels at

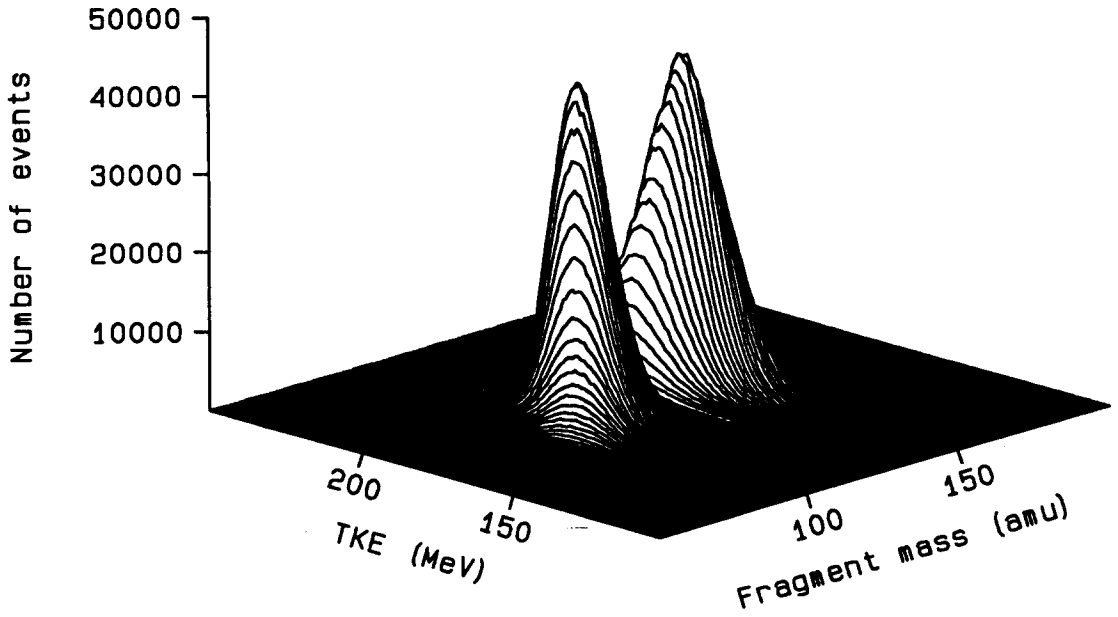

Fig. 1: Number of recorded events as a function of fragment mass (A) and total kinetic energy (TKE).

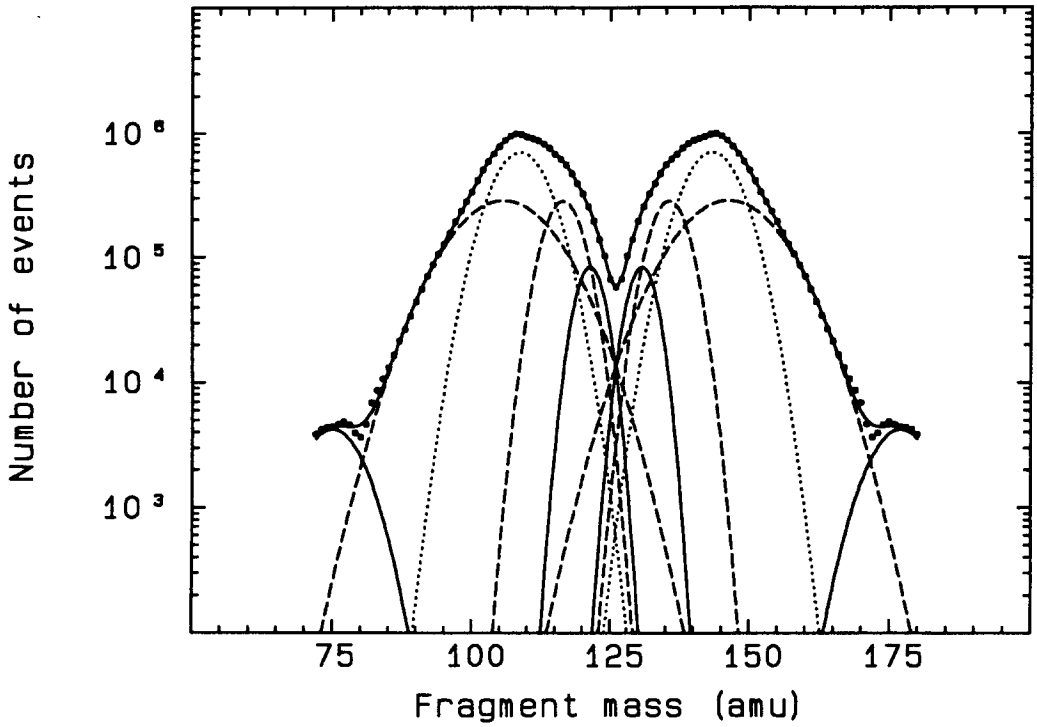

Fig. 2: Fission-fragment mass distribution.

the flanks of the distribution. The projection of the data (number of events as a function of fragment mass (A) and total kinetic energy (TKE)) onto the mass axis yields the fission-fragment mass distribution which is given in Figure 2. The humps around masses 77 and 175 may possibly originate from the superasymmetric fission channel but they also might contain fission fragments which have lost energy due to scattering. The best fit for the resolution of this distribution has been obtained with five gaussian functions for both the light and heavy mass regions. The positions of four of the gaussian functions are in good agreement with the average masses $<A_H>$ of four of the six fission channels predicted by the multi-modal random neck-rupture model, namely the three standard channels as well as the superasymmetric fission mode. The remaining two fission modes (supershort and superlong) are both expected to have average masses around $<A_H> \approx 127$ and are probably included in the fifth component.

The fission-fragment mass distributions for all experimental neutron multiplicities ($0 \leq \nu_{exp} \leq 9$) were also determined. From the resolution of the mass distribution for each neutron multiplicity ν_{exp}, we then obtained the areas of the gaussian distributions and also derived the neutron-multiplicity distributions corresponding to the various exit channels. Since we also measured the energies of the fragments, we obtained neutron-multiplicity distributions for every given mass as a function of TKE. From these partial neutron-multiplicity data, we iteratively obtained a three-dimensional array of the average neutron multiplicity $\bar{\nu}$ as a function of fragment mass (A) and total kinetic energy (TKE), which is displayed in Figure 3. The well-known sawtooth structure of the

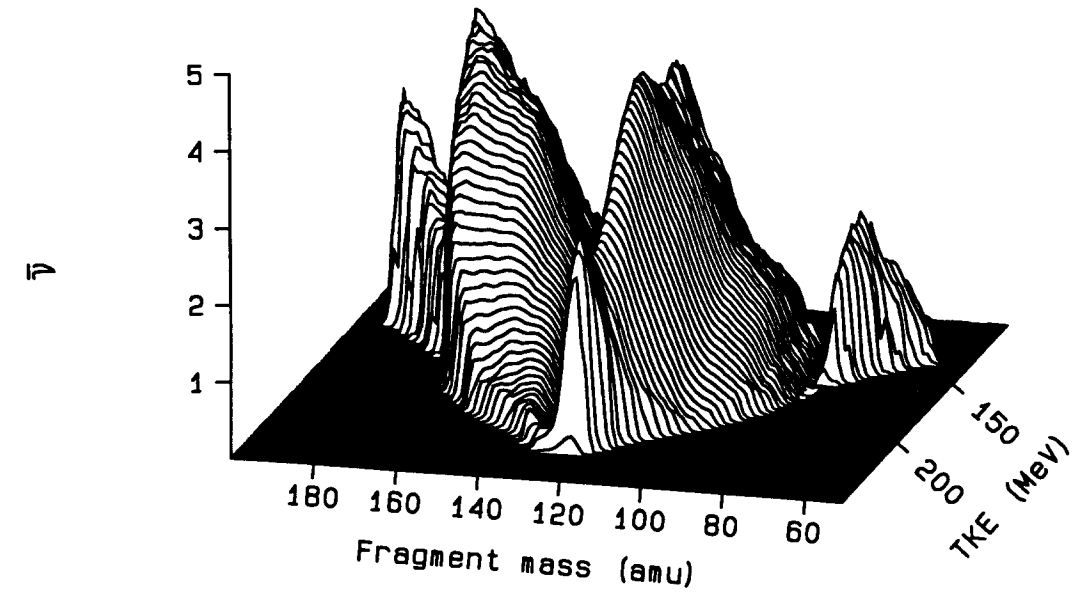

Fig. 3: Average neutron multiplicity $\bar{\nu}$ as a function of A and TKE.

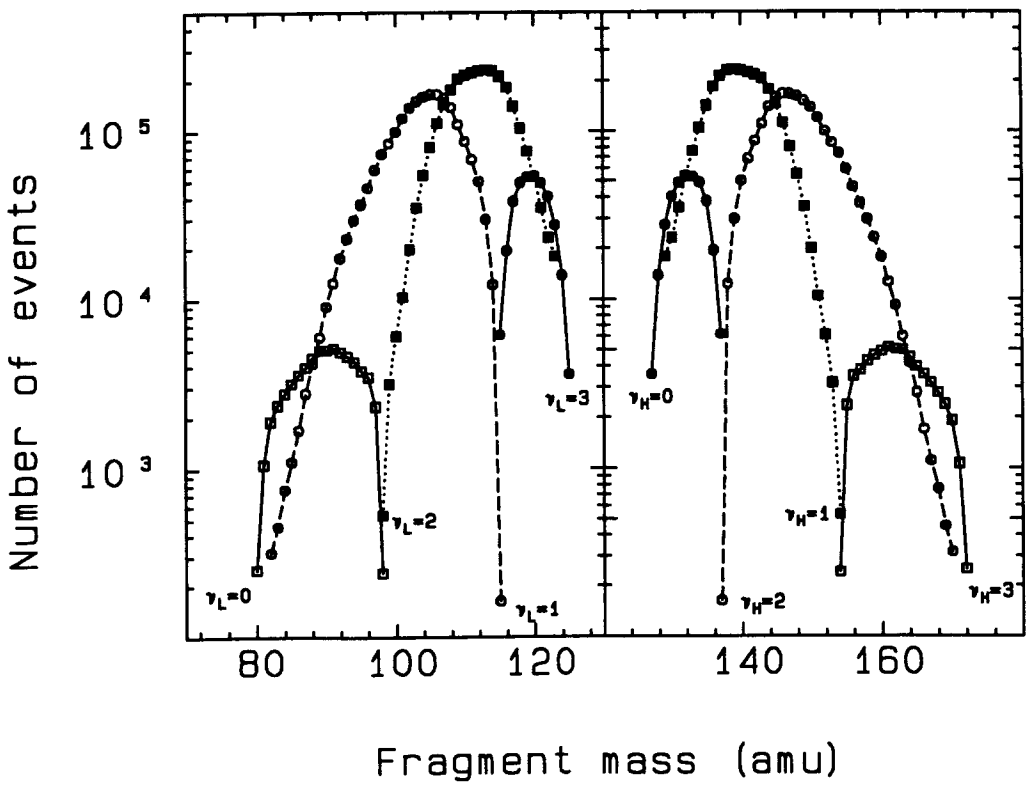

Fig. 4: Fission mass distributions for various partial neutron multiplicities, derived from fission events with a total number of three detected neutrons.

average neutron multiplicity $\bar{\nu}$ as a function of the fragment mass is found for all values of TKE. In addition, the figure shows some interesting structure. In the mass and TKE region where the superasymmetric fission channel is expected ($<A> \approx 73$ amu and $<A> \approx 179$ amu with $<TKE> \approx 140$ MeV), a third and a fourth sawtooth appear. In the mass region $120 \leq A \leq 130$ amu with TKE values around 230 MeV, we find values of $\bar{\nu}$ which are higher than expected from theoretical calculations. Fission events in this mass and TKE region are probably due to the supershort fission channel as proposed by Brosa. We have also constructed fragment mass distributions corresponding to various partial neutron multiplicities for a given experimental neutron multiplicity ν_{exp}. For the case of a total number of three detected neutrons, Figure 4 depicts the mass distributions of spontaneous fission events corresponding to various possible partial neutron multiplicities.

In addition, from the mass distributions corresponding to various partial neutron multiplicities of fission events with a given total neutron multiplicity, we have schematically derived various prescission configurations of the ^{252}Cf nucleus. The differences in these prescission configurations originate mainly from the length of the neck, and thus determine the deformation of the fission fragments immediately before and after neck rupture. The deformation according to these schematical pre-scission configurations can be expressed in terms of both TKE and mass increments. With these data, it may be possible to deduce the actual prescission shape of a ^{252}Cf nucleus for any given value of the total or even the partial neutron multiplicity.

§ To be published in Nuclear Physics A.

TECHNISCHE UNIVERSITÄT MÜNCHEN
FRM
FACHBEREICH PHYSIK

Coherent Neutron Scattering lengths and Total Cross Sections

Interaction of slow neutrons with nuclides of scandium, titanium, vanadium and manganese

L. Koester, K. Knopf, W. Waschkowski

Total cross section measurements at various neutron energies were performed on metallic and oxide samples of natural Sc, Ti, V, and Mn. By means of the Christiansen filter technique the coherent scattering lengths were determined on natural and isotopically enriched samples of Ti-, V-, and Mn-compounds. From the measured values we deduced the following data:

- the absorption cross sections (at 0.0253 eV in barn) of ^{nat}Ti (6.43 $\pm$ 0.06) and of ^{nat}V (5.06 $\pm$ 0.04);
- the bound coherent scattering lengths (in fm) of ^{nat}Ti (-3.370 $\pm$ 0.013), ^{46}Ti (4.72 $\pm$ 0.05), ^{47}Ti (3.53 $\pm$ 0.07), ^{48}Ti (- 5.86 $\pm$ 0.02), ^{49}Ti (0.98 $\pm$ 0.05), ^{50}Ti (5.88 $\pm$ 0.10), ^{nat}V (- 0.443 $\pm$ 0.014), and Mn (- 3.750 $\pm$ 0.018);
- the free potential radii (in fm) of Sc (3.60 $\pm$ 0.10), ^{46}Ti (3.50 $\pm$ 0.10), ^{47}Ti (3.60 $\pm$ 0.10), ^{48}Ti (3.90 $\pm$ 0.10), ^{49}Ti (4.10 $\pm$ 0.15), ^{50}Ti (4.50 $\pm$ 0.15), ^{51}V (5.20 $\pm$ 0.20), and Mn (6.50 $\pm$20).
- On the basis of the well known resonance parameters in combination with new fits of bound levels the spin state scattering lengths, the spin incoherence, and the obtained potential radii are discussed. Total cross section calculations were performed by multi-level formalism and are compared with the measurements.

Z. Phys. A 345, 175-182 (1993)

PHYSIKALISCH-TECHNISCHE BUNDESANSTALT BRAUNSCHWEIG

1. Neutron Data

1.1 Measurement of the $^{59}Co(n,p)^{59}Fe$ Cross Section between 8 and 14 MeV

W. Mannhart, D. Schmidt, Xia Haihong *

Measurements of the cross section for the $^{59}Co(n,p)^{59}Fe$ reaction were carried out at 19 neutron energies betweeen 8.10 and 14.32 MeV. The neutrons were produced via the $D(d,n)^3He$ reaction. Metallic cobalt foils 10 mm in diameter and 1 mm thick were attached to a low mass fission chamber with a ^{238}U deposit acting as a neutron fluence monitor. The samples were irradiated at zero degrees with a distance of 6 cm between the gas target and the samples. Corrections were applied for complementary neutrons from the D(d,np) breakup reaction [1], for neutrons scattered from the empty gas cell and for geometry effects.

Radioactivity counting was done with a calibrated HPGe detector. Both gamma-ray branches of ^{59}Fe were analyzed: 1099.3 keV with (56.1 ± 1.2)% and 1291.6 keV with (43.6 ± 0.8)%. The decay data were taken from Ref. [2].

In Fig. 1 the final data are shown in comparison with the ENDF/B-VI evaluation. The present data are the first available data set between 10 and 13.5 MeV and are substantially higher than the ENDF/B-VI evaluation. Between 8 and 13 MeV the ratio of the experimental data to the ENDV/B-VI evaluation is given by a constant factor of 1.169 ± 0.012 ($\chi^2/f = 0.84$).

Despite the large uncertainties (~ 2%) of both gamma-ray branches, a systematic trend dependent on the gamma-ray branch analyzed was identified. The cross sections measured via the 1099.3 keV branch were higher by a factor of 1.036 ± 0.010 ($\chi^2/f = 0.57$) than those obtained via the 1291.6 keV branch. This constant factor indicates an unsolved inconsistency in the decay data available. The cross sections shown in Fig. 1 are finally based on the 1099.3 keV branch parameters.

* Permanent address: CIAE, Beijing, P.R. China

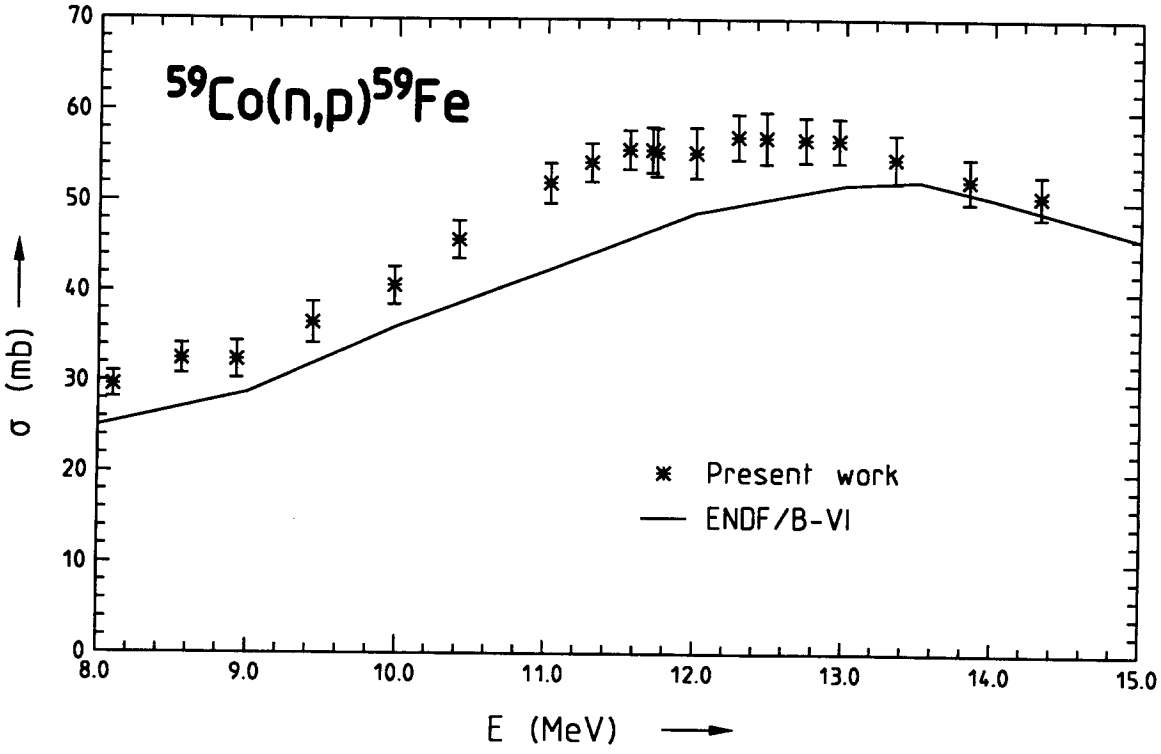

Fig. 1 Cross section data for the ^{59}Co(n,p)^{59}Fe reaction and comparison with the ENDF/B-VI evaluation.

1.2 Neutron Scattering from Natural Lead

D. Schmidt, W. Mannhart, Xia Haihong*

Neutron scattering measurements have been performed at eight incident energies between 8 and 14 MeV using a natural lead sample. Because the inelastic scattering in the neighbourhood of the elastic line is small (several percent of the elastic scattering at excitation energies between 0.6 MeV and 2 MeV), a minor influence on the elastic cross section derived is expected.

In these measurements, a low neutron detection threshold was used (< 1 MeV) in order to detect the main part of the neutron continuum. The contamination of the scattered TOF spectra by the scattered breakup neutrons will be corrected using realistic Monte Carlo simulations as proposed in Ref. [3].

Besides the DD neutron source, a ^{4}He(d,np) pure breakup source was also used in the scattering experiments. This should make an improved breakup correction possible as outlined in Ref. [4].

1.3 Neutron Production from the Deuteron Breakup on ^{4}He

D. Schmidt, Xia Haihong*

The DD reaction is a neutron source frequently used in the energy range below 14 MeV. However, in some cases the deuteron breakup continuum restricts the use of such a source. In scattering experiments in particular, the fractions of the scattered breakup neutrons cannot be separated. It is possible to overcome this problem with a realistic Monte Carlo simulation and its subtraction from the experimental spectrum. This method has been applied to correct the neutron scattering on carbon [3].

The quality of such a procedure depends on the reliability of the cross sections used in the simulation, most of which have been taken from an evaluation. However, an experimental correction of the scattered breakup neutrons using a pure breakup source is not easy to perform, because the shape of other pure breakup spectra, for instance from H, ^{3}He, ^{4}He ..., differs from that of the deuteron breakup on deuterium. By combining the two methods - scattering experiments with a deuterium and a ^{4}He source and simulation calculations for both measurements - the correction procedure can be substantially refined.

The measurements were carried out with the PTB's TOF spectrometer, under conditions similar to those described in Ref. [1]. The mean flight path of the measuring detector (diameter 4", thickness 1") was 12 m, the gas target length was 3 cm.

Two detection thresholds were used and, by means of a calibration with gamma sources, set to 150 keV (hardware threshold) and 480 keV (software threshold) electron energy equivalent. The californium method [5] was used to determine the thresholds, which were 0.884 MeV and 1.82 MeV in the neutron energy scale. The same gas target was used for the measurements with deuterium and helium. In separate measurements the linearity of the piezoelectric pressure sensor was checked and found to be better than 1% (in the pressure region between 1000 and 1900 mbar). The decrease in the gas density in the beam region due to gas heating was also studied; the influence of this effect on the cross section determination is in the order of less than 1%.

The mean deuteron energy was determined via the mean neutron energy of the DD neutrons derived from the TOF spectra. Since the energy loss of the deuterons in helium and deuterium differs by less than 10 keV in the energy region investigated, the same deuteron energy scale as that derived from deuterium was used for the helium measurement.

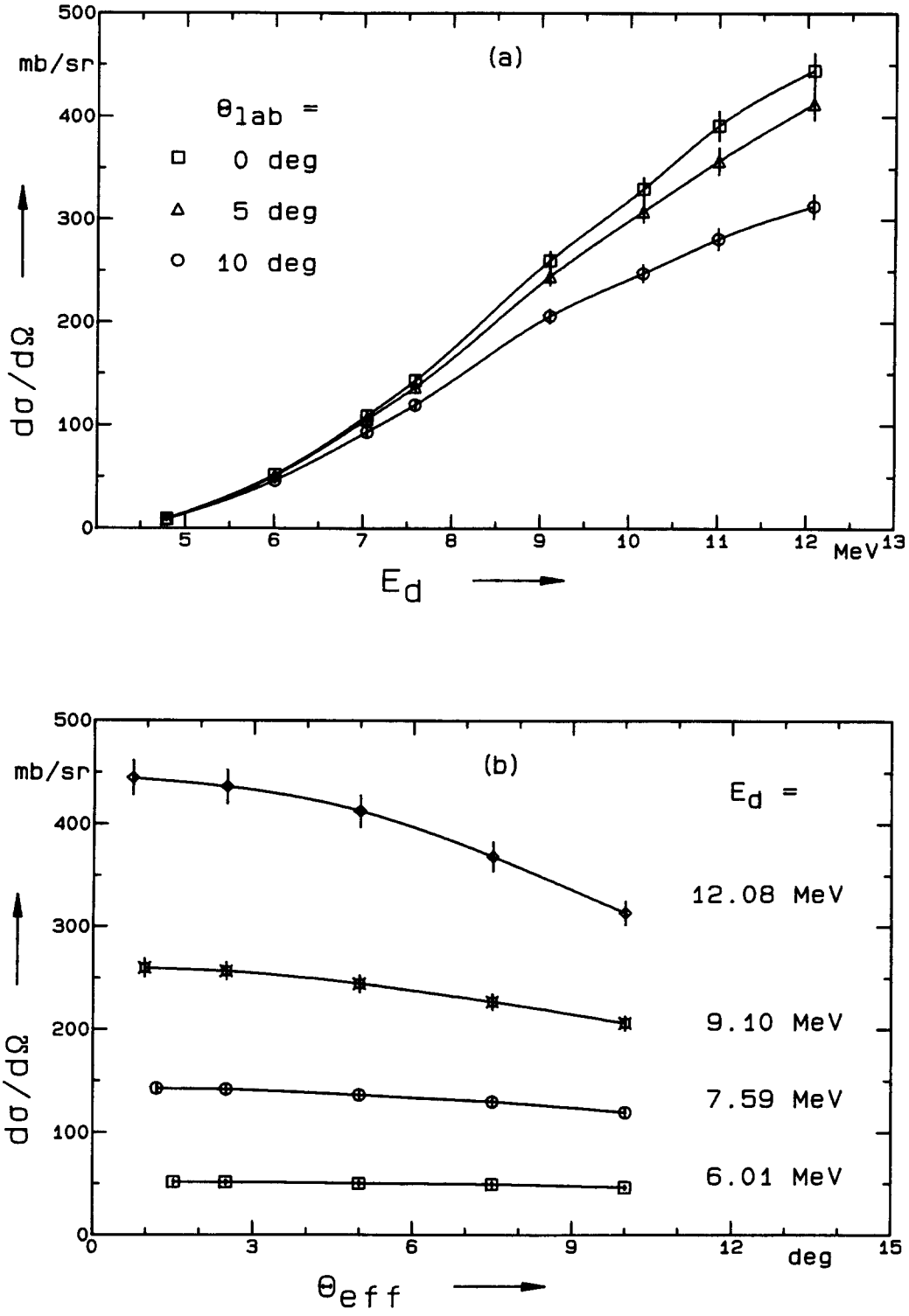

Fig. 2 Energy-integrated neutron cross sections of the deuteron breakup on ^{4}He (a) as excitation functions at different angles (detector position θ_{lab}) and (b) as angular distributions at different projectile energies E_d (the effective emission angles θ_{eff} were calulated using the SINENA code [7]); the curves are spline fits through the data points.

After correction of the TOF spectra for dead time and satellite pulses, subtraction of the gas-out spectra, renormalization to the same pressure, transformation to a linear energy scale and division by the efficiency curves, the spectra were absolutely normalized using the well-known cross sections of the DD reaction [6]. The neutron energy spectra below 1 MeV were extrapolated to zero by a quadratic function. More details are given in Ref. [4]. Fig. 2 shows the energy-integrated neutron cross sections of the deuteron breakup on ^{4}He as excitation functions (a) and as angular distributions (b).

1.4 Analysis of the Gamma Ray Production in a Gas Target

D. Schmidt, Xia Haihong*

In neutron time-of-flight (TOF) spectrometry the TOF line due to photons promptly emitted from the target is generally used as a reference point for the time. In a gas target, however, neutrons and gamma rays are produced at different loci, and the distance between the neutron and gamma lines must be corrected for this difference.

To determine the correction of the gamma line position, it is necessary to measure the gamma ray fractions emitted from the backing and from the foil of the gas target. The foil measurement inevitably includes the backing component, which must be subtracted to take the different energies at the "backing" and the "total" (backing and foil) measurements into account.

The use of a special target assembly allows the foil and the backing to be moved, under vacuum, into the beam region or out of it. The foil and the backing are mounted on iron plates, which can be moved from outside the assembly by means of a magnet. If both the foil and the backing are removed, the beam hits a solid target (TiD on silver). The same geometry (diameter of backing and foil, their distance) is chosen as in the normal gas target.

Because of its special construction, the target assembly has a considerable amount of iron near the backing and also near the foil. It was proved in two additional tests that no additional gamma rays occurred due to the interaction between self-target neutrons and the iron.

The TOF measurements were carried out using the PTB's TOF spectrometer [8]. The flight path between the solid target and the zero degrees detector was 12 meters. The hardware threshold of this detector was set to 0.3 MeV equivalent electron energy, but data acquisition also recorded spectra at software thresholds of 0.5, 0.7 and 0.9 MeV. The threshold of a second monitor detector at 60.4 deg was set to 0.5 MeV. This allowed the dependence of the correction on different thresholds to be studied as well.

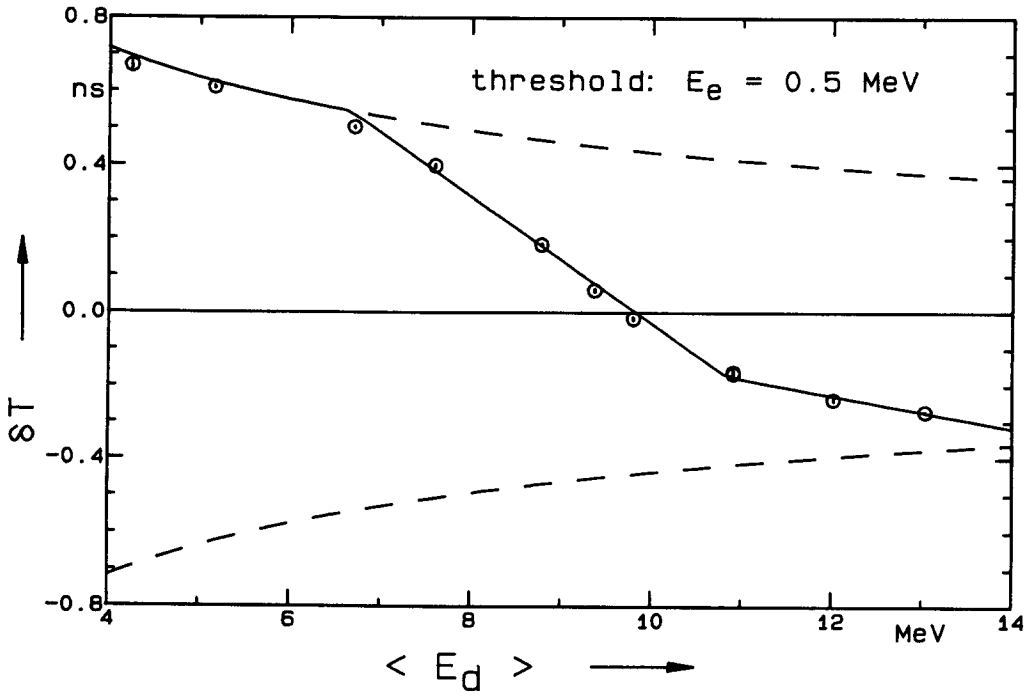

Fig. 3 Correction δT as a function of the averaged deuteron energy $<E_d>$; solid line: connection of the measured values for interpolation; dashed lines: correction if the photons were emitted only from the foil (top) or only from the backing (bottom).

The time correction δT is derived in such a way that the gamma emission is time-related to the centre of the gas target: the experimental gamma line position ch_γ (in channel) must be corrected to ch_γ - δT /TC, where TC stands for the time calibration value in units of ns/ch. The correction δT is calculated by two different methods.

In the first method, the yields (line area) of both fractions (from foil and backing) are used, whereas in the second method only their position on the time scale (centre-of-mass) is taken. Both methods furnish corrections which are in good agreement. The dependence of the correction δT was also studied for different emission angles and detection thresholds. For more details see Ref. [9].

Fig. 3 shows the correction δT as a function of the averaged deuteron energy $<E_d>$ (at the target centre, gas pressure 2 bar). Note that this correction is only valid for the given gas target construction (length 3 cm, 5 μm molybdenum foil, 0.5 mm gold backing).

2. Radionuclide Data

2.1 Gamma and X-Ray Emission Probabilities

U. Schötzig

Gamma- and X-ray emission probabilities per decay of ^{103}Ru have been derived from emission rates measured with Ge and Si(Li) detectors, and the activity determined with the $4\pi\beta$-γ coincidence technique [10]. Results are summarized in Table 1; uncertainties (in parentheses in terms of the last digit) correspond to one standard deviation. The sum of the X-ray emission probabilities $p_K = p_{K\alpha} + p_{K\beta1'} + p_{K\beta2'} = 0.0854(12)$ per disintegration of ^{103}Ru, taken from Table 1 has been converted by correction calculations to one disintegration of ^{103}Rh^m, yielding $p_k = 0.0766(14)$.

Table 1: Emission probabilities p

Nuclide	Energy [keV]	Radiation	p
^{103}Ru	20.17	Rh-K_α	0.0707(11)
	22.7	Rh-$K_{\beta1'}$	0.01248(21)
	23.2	Rh-$K_{\beta2'}$	0.00222(5)
	39.76	γ	0.000707(26)
	53.28	γ	0.00384(5)
	294.98	γ	0.00293(8)
	443.80	γ	0.00341(5)
	497.08	γ	0.911(8)
	557.04	γ	0.00844(9)
	610.33	γ	0.0564(5)

2.2 Half-Lives

H. Siegert

The half-life value $T_{1/2}$ of ^{121}Te was determined from count rate measurements with an HPGe detector by following the radioactive decay of ^{121}Te, which was a contaminant in an ^{123}I solution. The measurements were started after the ^{123}I had completely decayed. As result we obtained

$$T_{1/2} = 19.40(10) \text{ d.}$$

References

[1] S. Cabral et al.: Nucl. Sci. Eng. **106** (1990), p. 308

[2] U. Schötzig, H. Schrader: Report PTB-Ra-16/4, PTB Braunschweig/FRG (1993)

[3] D. Schmidt et al.: Report PTB-N-14, PTB Braunschweig/FRG (1993)

[4] D. Schmidt et al.: "Neutron Production from the Deuteron Breakup on ^{4}He", to be published

[5] J. Cub et al.: Nucl. Instrum. Meth. **A274** (1989), p. 217

[6] M. Drosg et al.: Handbook on Nuclear Activation Data, Technical Report Series No. 273, IAEA (1987), p. 83

[7] B.R.L. Siebert et al.: Report PTB-ND-23 (1982)

[8] R. Böttger et al.: Nuclear Data for Science and Technology, ed.: K.H. Böckhoff, Reidel Publ. Comp. Dordrecht (1983), p. 836

[9] D. Schmidt et al.: PTB-report, to be published

[10] U. Schötzig: to be published in Appl. Radiat. Isot. (1994)

APPENDIX

Addresses of Contributing Laboratories

Institut für Kernphysik III
Director: Prof. Dr. G. Schatz
Senior reporter: Dr. F. Käppeler
Kernforschungszentrum Karlsruhe
Postfach 36 40
76021 Karlsruhe

Institut für Kernphysik
Arbeitsgruppe Strahlungstransport
Senior reporter: Dr. D. Filges
Forschungszentrum Jülich
Postfach 1913
52425 Jülich

Institut für Nuklearchemie
Director: Prof. Dr. G. Stöcklin
Senior reporter: Dr. S.M. Qaim
Forschungszentrum Jülich
Postfach 1913
52425 Jülich

Institut für Kern- und Teilchenphysik
Director: Prof. Dr. H. Freiesleben
Senior reporter: Prof. Dr. K. Seidel
Technische Universität Dresden
Mommsenstr. 13
01062 Dresden

Zentrum für Strahlenschutz und Radioökologie
Head and senior reporter: Prof. Dr. R. Michel
Universität Hannover
Am Kleinen Felde 30
30167 Hannover

Abteilung Nuklearchemie
Director: Prof. Dr. G. Stöcklin
Senior reporter: Dr. U. Herpers
Universität zu Köln
Otto-Fischer-Straße 12 - 14
50674 Köln

Institut für Kernchemie
Director: Prof. Dr. G. Herrmann
Senior reporter: Prof. Dr. H.O. Denschlag
Universität Mainz
Fritz-Strassmann-Weg 2
55128 Mainz

Fachbereich Physikalische Chemie
Kernchemie
Senior Reporter: Prof. Dr. P. Patzelt
Philips-Universität Marburg
Lahnberge
35043 Marburg/Lahn

Fachbereich Physik
FRM
Senior reporter: Dr. W. Waschkowski
Technische Universität München
85747 Garching

Physikalisch-Technische Bundesanstalt
Abteilung 7, Neutronenphysik
Director: Prof. Dr. R. Jahr
Senior reporter: Dr. W. Mannhart
Bundesallee 100
38116 Braunschweig